




Cite this: RSC Adv., 2025, 15, 31723

# Plasmonic sensing in microfluidic paper-based analytical devices integrated with metal nanoparticles: a review

Priyamvada Venugopalan, <sup>\*a</sup> Shafeek Abdul Samad, <sup>a</sup> Nityanand Kumawat <sup>a</sup> and Sunil Kumar <sup>ab</sup>

Metal nanoparticles (MNPs) have emerged as vital components in nanotechnology due to their unique ability to concentrate light at the nanoscale. This property makes them especially valuable in biosensing applications, where high sensitivity is essential. At the same time, cellulose-based materials like paper offer an affordable, widely available, and versatile platform, making them ideal for the development of paper-based microfluidic analytical devices ( $\mu$ PADs). These devices are revolutionizing point-of-care testing and on-site detection due to their scalability, portability, and biocompatibility. The synergy between the three-dimensional versatility of paper and the optical prowess of MNPs, has given rise to cutting-edge nanodevices that satisfy the ASSURED criteria—affordable, sensitive, specific, user-friendly, rapid and robust, equipment-free, and deliverable to end-users. This review provides a comprehensive examination of both plasmonic and non-plasmonic roles of MNPs within  $\mu$ PADs. It explores various detection strategies enabled by MNP integration, including colorimetric, surface-enhanced Raman scattering (SERS), chemiluminescent (CL), electrochemical, and electrochemiluminescent (ECL) methods. For each technique, the basic principles, practical implementation, and analytical strengths and limitations are discussed in the context of paper-based sensing platforms. Special attention is given to SERS-based  $\mu$ PADs, which offer rapid, sensitive, and low-volume analysis, with growing potential due to advances in portable Raman instrumentation. By addressing both plasmonic and non-plasmonic functionalities of MNPs, this work aims to provide a comprehensive perspective on the future of nanoparticle-integrated  $\mu$ PADs in global healthcare and analytical science. Additionally, the review highlights the importance of paper-based device architectures in supporting the integration of MNPs, ultimately enabling next-generation diagnostic and sensing platforms for diverse applications.

Received 20th March 2025

Accepted 28th July 2025

DOI: 10.1039/d5ra01972a

rsc.li/rsc-advances

<sup>a</sup>Division of Engineering, New York University Abu Dhabi, Abu Dhabi, P.O. Box 129188, United Arab Emirates. E-mail: pv33@nyu.edu

<sup>b</sup>Department of Mechanical Engineering, New York University, Brooklyn, NY 11201, USA



Priyamvada Venugopalan

Priyamvada Venugopalan is a Research Associate in the Faculty of Engineering at New York University Abu Dhabi (NYUAD). She received her PhD in Physics from Swinburne University of Technology, Australia, in 2015. Her research spans plasmonic sensing, super-resolution imaging, and paper-based microfluidic analytical devices ( $\mu$ PADs), with her current work focusing primarily on advancing nanoplasmonics

in  $\mu$ PAD technologies. She has contributed to the development of 2D nanomaterial-based plasmonic structures aimed at improving the sensitivity and performance of optical sensing platforms.



Shafeek Abdul Samad

Shafeek Abdul Samad is a Post-doctoral researcher in the Division of Engineering at New York University Abu Dhabi (NYUAD). He received his PhD in Electrical Communication Engineering from the Indian Institute of Science (IISc), Bangalore, India, in 2023. His research focuses on the design and development of integrated photonic and plasmonic devices. He is a member of the IEEE Photonics Society and the Optica (formerly OSA).



# 1. Introduction

Over the past decade, there has been significant progress in developing portable biosensors that provide rapid and cost-effective clinical assessments, serving as diagnostic tools for disease screening, environmental monitoring *etc.*<sup>1</sup> Despite the significant enhancements in traditional analytical tools, the practical deployment of biosensors remains constrained by the need for sophisticated instruments, intricate sample preparations, and skilled technicians, which hinders their accessibility for rapid point-of-care (POC) testing.<sup>2</sup> In response to these challenges, there has been a concerted push towards developing user-friendly, economical, and reliable POC platforms.<sup>3</sup> Paper-based biosensors have emerged as an optimal solution, for health screening and POC testing, offering an ideal blend of performance, affordability, and ease of use, particularly in resource-limited environments prevalent in developing nations.<sup>4</sup> The versatility of paper as a flexible, porous, and biodegradable material has unlocked its potential in the realms of sustainable biosensors, bioelectronics, and beyond, where straightforward fabrication and operation are crucial.<sup>5,6</sup> Paper-based biosensors can be categorized into dipstick assays,<sup>7</sup> lateral flow assays,<sup>8</sup> microzone plates<sup>9</sup> and  $\mu$ PADs (microfluidic paper-based analytical devices).<sup>10</sup> The  $\mu$ PADs, in particular, combine the benefits of paper substrates with microfluidic technology, creating hydrophobic channels within hydrophilic paper. These devices stand out for their affordability and passive fluidic propulsion, requiring no pumps or external power sources. Moreover, they demand minimal sample volumes and are capable of multiplexed and quantitative analysis, overcoming the limitations faced by other methods.<sup>11</sup>

The incorporation of metallic nanomaterials into cellulose fibers introduces novel functionalities in paper-based biosensing platforms, particularly by exploitation of the interactions with light.<sup>4</sup> A prominent category of such nanomaterials is

gold nanoparticles (AuNPs), due to their distinctive optical properties, stability, and compatibility with biological functionalization.<sup>12,13</sup> Silver nanoparticles (AgNPs) are similarly employed since they can be obtained in different shapes and have a high extinction coefficient.<sup>14</sup> These metallic nanoparticles (MNPs) are particularly valued for optical detection methods, because of their strong light absorption and scattering, as well as their ability to generate intense local electric fields through localized surface plasmon resonance (LSPR).<sup>15</sup> This optical versatility of plasmonic nanoparticles is highly advantageous for various detection strategies, such as colorimetric sensing, which offers a simple visual readout directly on the  $\mu$ PAD.<sup>16,17</sup>

The scope of this review is to provide a comprehensive exploration of plasmonic and non-plasmonic aspects of MNPs within  $\mu$ PADs. Several reviews to date have examined  $\mu$ PADs, focusing on aspects such as fabrication methods, device design modifications, and their expanding range of applications.<sup>18</sup> These include uses in clinical diagnostics, environmental monitoring, food safety, and chemical analysis, with critical developments covering areas like assay integration, multistep reaction handling, and point-of-care deployment.<sup>19,20</sup> However, while these reviews provide a broad overview of  $\mu$ PAD technologies, plasmonics in paper-based devices remains an underexplored area, with only one prior review specifically addressing this topic.<sup>21</sup> To bridge this gap, the present review focuses on the foundational principles of plasmonics and the advanced sensing mechanisms enabled through the integration of MNPs into  $\mu$ PADs. Special attention is given to plasmonic sensing strategies, particularly Surface-Enhanced Raman Scattering (SERS) based applications due to their effectiveness and prevalence in this area.<sup>22</sup>

Furthermore, this review expands beyond just the optical properties of MNPs to discuss their non-plasmonic properties and how they can be leveraged in  $\mu$ PADs. These crucial non-



**Nityanand Kumawat**

*Nityanand Kumawat is a research scientist at New York University Abu Dhabi, where he leads research at the intersection of optical sensing, nanotechnology, and nanomaterials, leveraging techniques such as diffractive interferometry and plasmonics to achieve sensitive and selective detection of biomolecules. He also focuses on translating laboratory innovations into practical, accessible technologies by designing point-*

*of-care diagnostic devices using paper-based microfluidic analytical platforms ( $\mu$ PADs). He earned his PhD from the Indian Institute of Science (IISc), Bangalore, where he developed a self-referencing interferometric technique for biosensing applications and studying real-time binding kinetics of biomolecules.*



**Sunil Kumar**

*Sunil Kumar is a Global Network Professor of Mechanical Engineering at New York University. His scholarly research focuses on the transport of light and thermal radiation, applied optics, microfluidics, thermal-fluid analysis, and applied mathematics. He was previously Dean of Engineering at NYU Abu Dhabi and Graduate Dean at NYU Tandon School of Engineering. He is a Fellow of the*

*American Society of Mechanical Engineers and a Member of the Mohammed bin Rashid Academy of Scientists.*



plasmonic characteristics include: high surface area to volume ratio, which enhances reactivity and interaction with other molecules, significant catalytic properties, especially in smaller MNPs (typically less than 5 nm), remarkable electronic properties, such as high thermal and electrical conductivity.<sup>23,24</sup> These non-plasmonic attributes make MNPs powerful tools in catalysis, electronics, and sensor technologies, further enriching the capabilities of paper-based analytical devices. In electrochemical, chemiluminescence, and electrochemiluminescence detection platforms, MNPs can enhance conductivity, increase surface area, introduce functional chemical groups, or serve as catalysts to amplify light or electrical signals.

This review begins with an introduction to both the plasmonic and non-plasmonic properties of MNPs in Section 2, laying the foundation for their roles in analytical applications. Section 3 delves into the fundamentals of paper substrates, discussing various types of paper and their relevance in microfluidic device fabrication. In Section 4, current techniques for the immobilization of MNPs onto paper substrates are explored, highlighting both solution-based and physical deposition methods. The review proceeds to examine a range of paper-based analytical platforms, including dipstick assays, lateral flow assays, microzone plates, and  $\mu$ PADs in Section 5. The underlying principles of each platform are briefly explained, emphasizing their enhanced performance when integrated with MNPs. A detailed focus on  $\mu$ PADs is provided in sub-Section 5.4, where the integration of MNPs is discussed in the context of enabling advanced sensing mechanisms. These include plasmonic sensing techniques, such as colorimetric detection, with particular attention to SERS in sub-Section 5.4.2, and non-plasmonic mechanisms, including chemiluminescence, electrochemical, and electrochemiluminescence sensing, covered in sub-Section 5.4.3. Section 6 summarizes the key findings, highlighting the unique advantages of MNP integrated  $\mu$ PADs in terms of sensitivity, portability, and potential for POC use. Finally, Section 7 addresses the critical challenges and future perspectives, particularly focusing on commercialization pathways, the need for standardization, and strategies to overcome translational bottlenecks.

Through this comprehensive overview, it becomes clear that MNP integrated  $\mu$ PADs represent a significant advancement in analytical technology. Positioned at the intersection of materials science, nanotechnology, and microfluidics, these platforms are paving the way toward the development of next-generation sensors for point-of-need applications, including lab-on-chip and lab-on-paper systems with broad potential across healthcare and environmental diagnostics.

## 2. Properties of metal nanoparticles

Metallic nanoparticles (MNPs), typically sized between 10 and 100 nanometers, exhibit unique properties that differ significantly from their bulk counterparts. These properties are broadly categorized into plasmonic and non-plasmonic types, both of which are highly dependent on the particle's size, shape, and surface characteristics.

A key feature of MNPs is their high surface area to volume ratio, which enhances their reactivity and interaction with other molecules.<sup>25</sup> This makes them highly suitable for applications in catalysis, drug delivery, and sensing. Additionally, their surfaces can be functionalized with specific molecules, allowing for targeted interactions, such as binding to ligands, drugs, or antibodies.<sup>26</sup> The optical, electronic, and catalytic behaviors of MNPs can be finely tuned through morphological control, making them versatile tools in nanotechnology. Their unique properties have enabled breakthroughs in fields ranging from medicine to environmental sensing. In the following sections, we explore in detail the plasmonic and non-plasmonic properties of MNPs, highlighting their mechanisms and applications.

### 2.1 Optical/plasmonic properties

When light is incident on a metal nanoparticle, the oscillating electric field displaces the free electrons at the surface of the nanoparticle with respect to the lattice ions.<sup>27,28</sup> This displacement generates a restoring force, leading to electron oscillations known as surface plasmons, whose frequency depends on the mass of the electrons and the magnitude of the restoring force (Fig. 1a(i-ii)).<sup>29</sup> When the frequency of incident light matches that of the surface plasmon, a localized surface plasmon resonance (LSPR) is created at the MNP surface creating extremely strong electromagnetic fields, or "hot spots". These hot spots are pivotal in amplifying light-matter interactions, an important concept in nanoplasmonics recognized for its universal significance.<sup>30,31</sup> Fig. 1a-ii illustrates the electric field distribution for various shapes of MNPs.

While silver and gold are the most commonly used materials, LSPR can theoretically occur in any metal, alloy, or semiconductor with a highly negative real dielectric constant and a low imaginary dielectric constant.<sup>33,34</sup> Near the surface of LSPR nanostructures, the electric field is significantly enhanced, which falls off quickly with increasing distance from the nanostructure. This means that the LSPR is a near-field effect, which requires coupling with the plasmon at a relatively short distance to be effective. LSPR can result in strong absorption, scattering, reflection, or transmission at specific wavelengths, which are highly influenced by factors such as the nanoparticle's composition, size, shape, orientation, and the surrounding dielectric environment.<sup>35,36</sup> The enhanced light absorption at the plasmon resonance frequency appears as a dip/peak in the optical transmission/reflection spectrum. This property can be leveraged in designing LSPR nanostructures to optimize light-solid interactions, especially for sensors that rely on light absorption.

Theories like Mie theory<sup>37,38</sup> and its Modified Long Wavelength Approximation (MLWA)<sup>39</sup> are commonly applied to explain the significant increase in absorption and scattering at resonance, as well as to calculate extinction spectra. The Drude model further explains how the surrounding dielectric constant influences the LSPR peak wavelength, revealing an approximately linear relationship between the LSPR peak wavelength and the refractive index.<sup>40</sup> This property enables high-sensitivity detection using LSPR-based sensors,<sup>41</sup> which are particularly



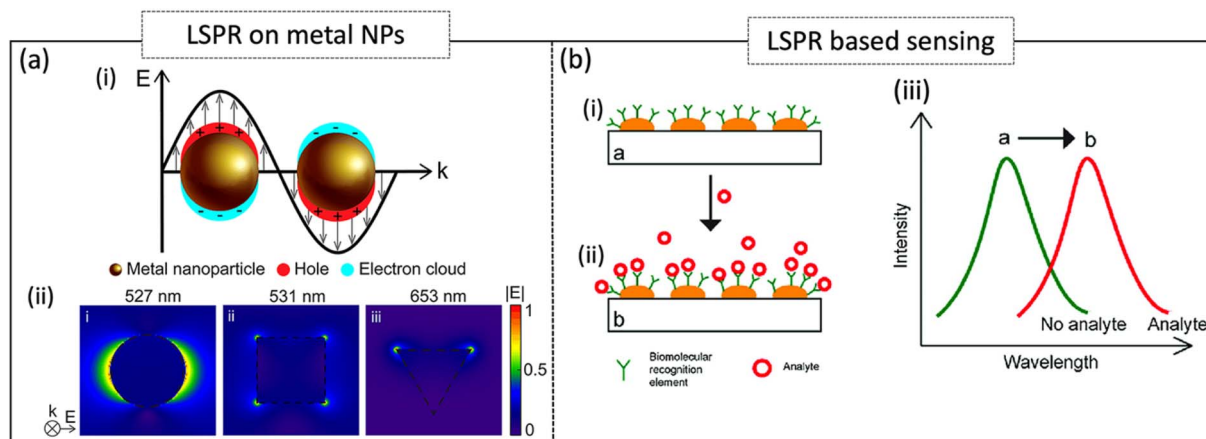


**Fig. 1** (a) Background of nanoplasmonics: (i) Scheme of the electron cloud oscillations, Finite difference time domain (FDTD) calculation of the normalized electric field distribution at the resonance wavelength of (ii-i) a nanosphere, (ii-ii) a nanocube, and (ii-iii) a nanotriangle. This figure has been adapted from ref. 29 with permission from AIP PUBLISHING, copyright 2021. (b) LSPR biosensing principle. (i) Biomolecular recognition elements (e.g., antibody) are immobilized on the surface of metal nanosubstrate, (ii) these elements capture analytes (e.g., antigens) from a liquid sample, causing a localized increase in the refractive index at the metal surface, (iii) this interaction results in a peak-wavelength shift in the extinction spectra. This figure has been adapted from ref. 32 with permission from Elsevier, copyright 2018.

effective in identifying analyte molecules through observable spectral shifts in NP extinction and scattering spectra.<sup>42,43</sup> Such shifts occur when molecules with higher refractive indices than the buffer solution bind to NPs, increasing the local refractive index and inducing a redshift in the spectrum<sup>32</sup> (Fig. 1b). LSPR also enables the detection of small target molecules *via* Surface-Enhanced Raman Scattering (SERS), where Raman signals are significantly amplified (by factors of  $10^4$  to  $10^8$ ) when the analyte is adsorbed near a MNP or roughened metallic surface. Additionally, colorimetric sensing, another class of optical detection, leverages the detection of spectral shifts (often towards longer wavelengths) when MNPs aggregate. This principle underpins widely recognized tools such as the home pregnancy test, highlighting the diverse applications of MNPs in diagnostics and sensing technologies.

The plasmonic properties in metal nanostructures has been capitalized upon in diverse fields, ranging from label-free biosensing,<sup>44</sup> cancer cure,<sup>45</sup> neuroengineering,<sup>46</sup> super-resolution nano focusing<sup>47</sup> and nearfield optical characterization.<sup>48</sup> Recent advancements in nanoplasmonics have paved the way for groundbreaking applications, including single molecule Raman probing,<sup>49</sup> ultrafast plasmonics,<sup>50</sup> plasmonic nano lasers<sup>51</sup> and photothermal conversion,<sup>52</sup> among others.

## 2.2 Non-plasmonic properties

In addition to their plasmonic behavior, MNPs also exhibit crucial non-plasmonic properties. They demonstrate significant catalytic properties, largely due to their high surface to volume ratio. Very active catalysts are typically produced when MNPs are less than approximately 5 nm and conversely, their activity diminishes considerably as particle size grows beyond 10 nm.<sup>23</sup> The reactivity and selectivity of these catalysts can be precisely controlled by manipulating the morphology of the nanocrystals.

Engineered metal nanocrystals are utilized as catalysts for various chemical transformations, including oxidation reactions,

carbon-carbon coupling, electron transfer, *etc.*, with some even having industrial-scale catalytic applications.<sup>24,53,54</sup> Maintaining the stability of these NPs and managing any surface coating agents are also critical considerations, as these can affect their shape, dimensions, lifespan, or even inactivate catalytic regions during reactions.<sup>23</sup> Their electronic properties are equally noteworthy, particularly the high thermal and electrical conductivity observed in certain metal nanocrystals such as silver nanowires and nanorods.<sup>55</sup> Remarkably, silver nanorods with a diameter of 20 nm can exhibit electrical conductivity twice that of bulk conductors. These nanocrystals combine small size with excellent thermal and electrical conductivity, enabling their use in a range of advanced electronic and sensing devices.<sup>56</sup> AuNPs and AgNPs have been successfully applied in chemiluminescence systems, where they act as catalysts to enhance light emission and improve detection sensitivity.<sup>57</sup> In electrochemical sensing, MNPs can be deposited onto electrodes to improve conductivity, enhance surface area, and introduce specific chemical functionalities.<sup>58</sup> Their large electrochemically active surface facilitates faster electron transfer, thereby increasing the sensitivity, selectivity, and response speed of sensors.

Overall, these non-plasmonic properties underscore the versatility of MNPs across various disciplines. Their tunable morphology, surface characteristics, and size-dependent behaviors make them powerful tools in catalysis, electronics, and sensor technologies. In the following sections, we focus on the integration of paper-based substrates with MNPs to create analytical tools that are not only simple and low-cost but also easy to fabricate, aligning with the needs of modern diagnostics and therapeutics.

## 3. Paper as a sensing substrate

Paper has been developed and used as a supporting material for over 1000 years. The remarkable attributes of paper, including





flexibility, thinness, low volume, and biocompatibility, are complemented by its ease of access and exceptional storage capacity.<sup>59</sup> Moreover, paper stands out in the market for its cost-effectiveness, being significantly more economical than alternative substrates. To illustrate, paper boasts a nominal cost of approximately 0.1 cent per square decimeter, whereas the plastic substrates polyethylene terephthalate (PET) and polyimide (PI) cost approximately 2 and 30 cent dm<sup>-2</sup>, respectively.<sup>60</sup> Therefore, compared to the devices made of silicon, glass or plastic substrates, paper-based devices have gained growing interest in POC applications.

Paper is made by compressing and chemically treating a dilute suspension of cellulose fibers.<sup>61,62</sup> Paper can be prepared from different raw materials, for example, wood (mainly for producing printing paper), cotton (for producing filter papers), flax, bamboo, grass, and straw *etc.*<sup>10</sup> But the high amount of lignin in wood adversely affects the paper durability<sup>63</sup> and thus papers made from only cotton are preferable in sensing applications.<sup>64</sup> By mechanical pressure, chemical or pre enzymatic treatments, cellulose fibers can be disintegrated to microfibrillated cellulose (MFC), cellulose nanofibrillated (CNF), cellulose nanocrystalline (CNC), among other cellulose materials.<sup>65</sup> MFC fibers are elongated hollow fibers isolated from tree *via* mechanical treatments under high temperature. CNC fibers are produced by acid hydrolysis of wood and plant fibers. It involves cooking the fibers to facilitate the removal of residual lignin, thereby yielding long, porous cellulose fibers. CNF is normally produced from wood pulp and plant fibers by combining mechanical processes with pre-enzymatic treatments.<sup>62,66</sup> A comprehensive analysis by Moon *et al.*, offers a succinct overview of cellulose materials, their properties and fabrication methods.<sup>67</sup> An innovative nanocellulose material, named bacterial cellulose (BC), is produced through the fermentation of sugar by Gram-negative bacteria, like *Gluconacetobacter xylinus* (reclassified from *Acetobacter xylinum*).<sup>68</sup> The cost of nanocellulose, however, can be higher than that of traditional cellulose materials, due to the specialized production processes that necessitate increased energy and material inputs.<sup>69</sup>

Paper substrates usually have a thickness of approximately 100  $\mu\text{m}$ , paired with a basis weight, or grammage, of about 80 gm<sup>-2</sup>. In the lighter end of the spectrum, when the grammage is within the 12–30 gm<sup>-2</sup> range, it is known as tissue paper. When the grammage exceeds 200–800 gm<sup>-2</sup> or when the thickness is larger than 300  $\mu\text{m}$  it is often referred to as paperboard or cardboard.<sup>70</sup> The properties of paper substrates are remarkably diverse, depending on the structure and composition. The inherent hydrophilicity of cellulose can cause challenges as the sample tends to spread out over a large area. However, this obstacle was overcome by exploiting the versatility of paper, which can be easily modified to exhibit a range of hydrophobic, strength, and physical characteristics through various coating and impregnation techniques. Paper's high surface area supports efficient loading and uniform distribution of metal nanoparticle, essential for sensitive detection. Solution-based methods such as inkjet printing, spray-coating, drop casting, *etc.* take advantage of paper's fibrous network to facilitate

effective immobilization of metal nanoparticles, while chemical modifications enhance nanoparticle adhesion. Even physical deposition methods benefit from paper's structure for dense nanoparticle stabilization. These strategies are explained in detail in Section 4 of this review. These modified cellulose products enable the creation of versatile, high-performance sensing platforms.<sup>71,72</sup> Paper substrates have been developed for a variety of cutting-edge applications, including electronic devices, digital displays, and photovoltaic devices.<sup>5,60</sup> Furthermore, paper substrates are utilized in the preparation of test paper or indicator paper; having successfully developed gas, pH, and temperature sensors on these versatile materials.<sup>73,74</sup>

## 4. Immobilization of metal nanoparticles on paper substrates

This section gives an overview of the key techniques for immobilizing or stabilizing metal nanoparticles (MNPs) on a paper substrate. The existing fabrication techniques can be categorized into (1) MNP deposition techniques (based on solution processing), and (2) material deposition under vacuum (physical deposition). We also discuss on the modification of paper by plasma treatment and surface functionalization for improved sensing characteristics.

### 4.1 Solution-based deposition methods

This section focuses on the fabrication of paper-MNP hybrid platforms based on solution processing, which is renowned for its efficiency in material and energy consumption. This approach has been widely recognized and reported by multiple research groups, underlining its significance in the field.

**4.1.1 Inkjet printing.** Inkjet printing offers precise control over MNP deposition, just by direct printing NP colloidal solutions on paper (Fig. 2a). Recent studies have demonstrated that inkjet-printed Au or Ag inks can result in enhanced Raman signals due to uniform NP distribution on the paper substrate. White's group reported an ultra-low-cost paper-based SERS substrate using a commercial piezo-based inkjet printer.<sup>75</sup> Zhigao Dai *et al.* fabricated highly reproducible SERS substrate based on inkjet printing Au nanorods on flexible paper substrates.<sup>76</sup> Paper-based devices made with inkjet printing can enable low-cost chemical and biomolecular detection in the lab as well as in the field at the point of sample collection.<sup>75,77</sup>

**4.1.2 Spray-coating.** This technique involves spraying a solution of MNPs onto the paper surface (Fig. 2b). It is useful for uniform coating over large areas and for scalable production. A disposable paper-based Au/Ag NP substrate was prepared through a straightforward spraying process that eliminates the need for complex procedures.<sup>78</sup> When optimized, these paper-based Au/Ag NP substrates exhibit consistent reproducibility, and remarkable long-term stability, making them particularly effective for the analysis of residual substances in fishery products.

**4.1.3 Drop casting.** Drop casting is a simple yet economical method that involves dropping a solution containing NPs onto a pre-cut piece of paper (Fig. 2c). After drying, the NPs remain



### Stabilization of Metal Nanoparticles (NPs) on Paper Substrates (Based on Solution Processing)

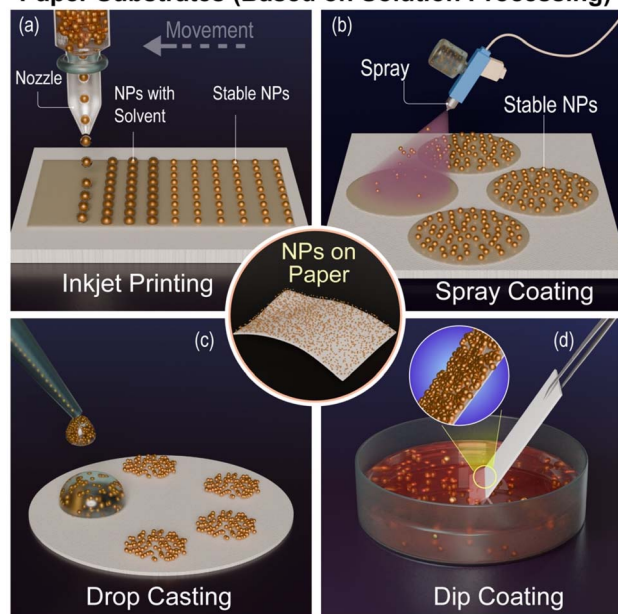


Fig. 2 Stabilization of MNPs on cellulose fibers by using solution processes (a) Inkjet printing: direct printing of Au and Ag nanoparticle inks on paper enables uniform nanoparticle distribution for low-cost chemical and biomolecular detection, (b) spray coating: applying a solution of MNPs onto the paper surface, offering a simple and scalable method for achieving uniform nanoparticle coverage, (c) drop casting: dropping a nanoparticle solution onto paper forms hybrid paper-MNP platforms upon drying, and (d) dip coating: immersing paper in nanoparticle solutions and withdrawing it deposits nanoparticles onto the fibers after drying.

on the surface and within the fibers of the paper, creating paper-MNP hybrid platforms.<sup>79</sup> This method is adaptable for different NP types and ideal for research and POC applications.<sup>80</sup> Limitations of drop-casting method are non-uniformity of NP distribution and possible aggregation, reducing signal consistency.

**4.1.4 Dip coating.** In this method, paper substrates are immersed in solutions having colloidal metal nanostructures with different morphologies, followed by withdrawal at a controlled speed (Fig. 2d). The substrate is then allowed to dry, leaving behind a layer of NPs adhered to the paper fibers.<sup>81,82</sup> While simple, scalable and cost-effective, this technique requires either nanoparticle's solutions in a rather high concentration, like for the printing method, or long dipping times (typically 24–48 hours) to obtain a sufficiently high loading. Chemical modification of paper fibers prior to dip coating has been demonstrated to enhance the adhesion and distribution of NPs.<sup>83</sup>

**4.1.5 Chemical reduction.** *In situ* synthesis of MNPs through chemical reduction involves soaking paper in a metal salt solution (e.g., AgNO<sub>3</sub>, HAuCl<sub>4</sub>), followed by reduction using agents like sodium borohydride.<sup>84,85</sup> This method is advantageous for producing uniform and highly dispersed MNPs directly on the paper, and is suitable for large-scale production.

In SERS applications, the background signal of non-SERS-active byproducts from the reagents used for the *in situ* growth of NPs and the fast oxidation rate of NPs have quenched the interest in these types of methods.<sup>86</sup>

### 4.2. Physical deposition methods under vacuum

Deposition techniques under vacuum allow for precise control over the thickness and distribution of materials, especially MNPs, onto the paper substrate. These techniques include physical vapour deposition (PVD), pulsed laser deposition *etc.*

**4.2.1 Chemical vapour deposition (CVD).** Plasma deposition, particularly atmospheric-pressure plasma-assisted CVD, has recently emerged as a simple and cost-efficient method for nanogold deposition. In this process, a plasma jet of high-density electrons reduces the gold solution (HAuCl<sub>4</sub>) into metallic gold, which is rapidly deposited onto the substrate without the need for additional reducing or stabilizing agents,<sup>87</sup> Fig. 3a. As plasma printing eliminates the need for complicated chemical steps or advanced electron or ion beam processing in vacuum conditions, it presents a promising alternative for fabricating paper-MNP hybrid platforms.

**4.2.2 Physical vapour deposition.** In PVD, metal sources are heated under high vacuum until they evaporate and condense onto the paper as shown in Fig. 3b. Zhang *et al.* presented the fabrication of highly efficient SERS test strips by PVD coating of Ag nanolayers on different kinds of papers containing natural wrinkle and fibril structures, where the latter formed a rough surface which could serve as SERS “hot spots”.<sup>88</sup> Highly dense and uniform distribution of MNPs are formed *in situ* during the thermal evaporation of ultra-thin (few nm) metal films (e.g. Ag, Au) onto heated (150 °C) paper substrates.<sup>89,90</sup> In the work reported by Araújo *et al.*, AgNPs were obtained by the deposition of metal layers directly on the cardboard substrate (2.5 × 2.5 cm<sup>2</sup>) using an electron gun-assisted thermal evaporation technique.<sup>91</sup> Araújo *et al.* demonstrated a three-dimensional hybrid SERS substrate using a simple and scalable two-step method.<sup>92</sup> Highly ordered ZnO NRs were grown directly on paper substrate using a microwave heating technique and made SERS-active by decorating them with a dense array of silver NPs deposited *via* a single-step thermal evaporation technique. The high concentration of AgNPs together with a high surface area makes this substrate an ideal candidate for SERS sensing system.

**4.2.3 Laser-induced deposition.** Laser-induced deposition involves focusing a laser beam on a target surface (in this case, paper) in the presence of a precursor material (Fig. 3c). The laser energy can be absorbed by the precursor, causing it to break down and deposit MNPs onto the surface. Au and Ag NP patterns are prepared on paper substrates by means of pulse-laser irradiation of a thick silver film (*via* laser-induced photo-thermal effect) that was initially deposited by sputtering.<sup>93</sup> These substrates pave the way for the colorimetric detection of biomolecules, enabling visual identification of color shifts with the naked eye. Using the same technique, Yu *et al.*, contributed to the development of an eco-friendly paper substrate with NPs. This substrate is created through a single-shot laser-induced photothermal effect, achieving Ag or Au NP formation with



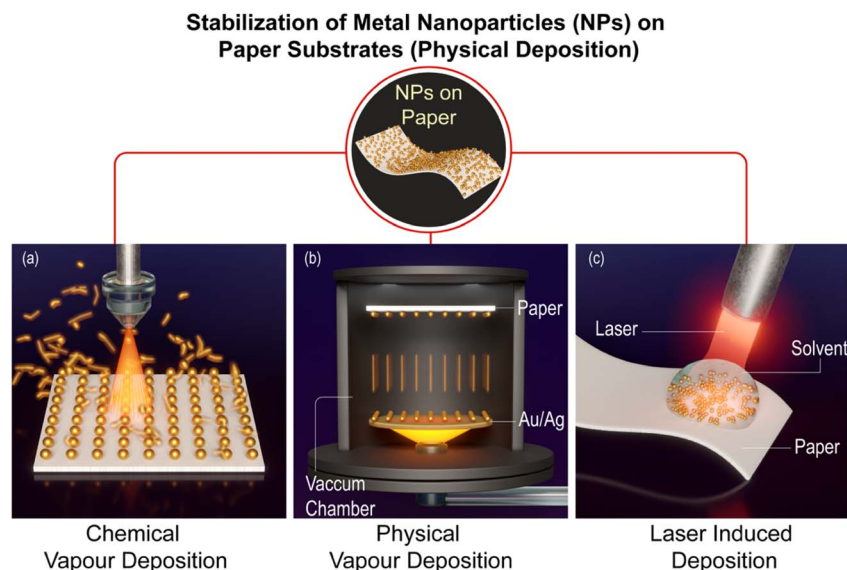


Fig. 3 Stabilization of MNPs on paper substrates by using physical deposition methods (a) chemical vapour deposition: uses a plasma jet to reduce gold solution and deposit nanoparticles directly onto substrates, (b) physical vapour deposition: metal sources are evaporated under high vacuum and condensed onto paper substrates, forming dense and uniform nanoparticle layers and (c) laser induced deposition: a focused laser beam decomposes precursor materials, depositing Au and Ag nanoparticles onto paper surfaces.

the potential for single fabrication, large-area processing, precise NP positioning, and the ability to form high-density NP arrays on paper substrates.

Physical deposition techniques require the use of high-power lasers, and precise temperature regulation to shape and organize NPs, which are often not suitable for paper-based substrates.<sup>93</sup> The need of expensive equipment in these techniques, hinders the large-scale production of low-cost sensing devices.

**4.2.4 Surface modification via nano functionalization.** Detection sensitivity is a big challenge in the development of a paper-based substrate. The fibril structures inherent in paper materials necessitate a suitable modification to enhance the bonding efficacy at the paper-metal interface. An optimization of surface conditions for metal nanostructures is crucial for achieving heightened sensing performance on paper.

**4.2.5 Plasma treatment.** Plasma treatment modifies the paper surface by creating functional groups that improve NP adhesion. Alder *et al.* has showcased the efficacy of direct plasma deposition in creating optimal surface conditions through the utilization of nanogold from a solution precursor.<sup>72</sup> This approach circumvents the common issue of contamination from residual chemicals, including reducing and stabilizing agents, ensuring an unadulterated finish.<sup>94</sup>

**4.2.6 Surface functionalization.** Functionalizing the paper surface with chemical groups (*e.g.*, thiols AuNPs) allows for better NP attachment, improving the stability of NPs on paper.<sup>95</sup> Wu *et al.*<sup>71</sup> designed and fabricated a functionalized filter paper consisting of gold nanorods functionalized with mono-6-thio-cyclodextrin (HS- $\beta$ -CD) (used as an inclusion compound to capture hydrophobic molecules) as a SERS substrate. This paper-based substrate is a promising material for the rapid,

direct, and sensitive detection of hydrophobic adulterants in herbal medicine.

## 5. Sensing mechanisms in paper-based devices integrated with metal nanoparticles

Paper-based analytical devices (PADs), that use paper as a substrate for sampling and detection, are more affordable and easier to produce, revolutionizing the diagnostic process.<sup>96</sup> PADs stand out not only for their cost-effectiveness and ease of production but also for their convenient storage, transportation, and eco-friendly disposal methods. In the cutting-edge field of lab-on-chip technology, the fusion of electronics and microfluidics is paving the way for innovative functions and devices.<sup>99</sup> Traditionally, the construction of these devices involves a complex process of layering electronic and microfluidic components, necessitating extensive steps in fabrication, assembly, and connectivity. However, the advent of lab-on-paper devices is revolutionizing the industry by harnessing cost-effective, scalable printing techniques on a versatile substrate.<sup>97</sup> Paper offers a compliant canvas for functionalization, such as embedding cellulose, forming hydrophobic barriers, and creating designated areas for biomolecules and reagents, and has natural microfluidic transport properties.<sup>98</sup>

Martin and Syngé reformed the separation of mixture components by pioneering the use of paper as a platform, a groundbreaking achievement that earned them the Nobel Prize in 1952.<sup>99</sup> Building on this robust foundation, paper has since become integral to a variety of analytical and bio-analytical applications.<sup>20</sup> Further advancing the field, Whiteside utilized paper for microfluidic applications, introducing



the innovative concept of Microfluidic Paper-based Analytical Devices ( $\mu$ PADs).<sup>100</sup> Today, a diverse array of papers—including chromatography paper, filter paper, nitrocellulose membrane paper, bioactive paper, graphite paper, glossy paper, vegetal paper, and flexible paper—stands at the ready to craft paper-based sensors. These materials are selected based on the specific fabrication technique, intended application, and target analyte, ensuring precision and adaptability in sensor design.<sup>10</sup>

The wicking capability of paper can be utilized to drive the sample flow without the need for external mechanical components. This is shown in the utilization of filter paper (Whatman 1) for analyte separation and identification, a technique named as “Paper Chromatography” that employs the inherent hydrophilicity of paper to facilitate passive sample flow.<sup>101</sup> The efficacy of this method is intrinsically linked to the cellulosic composition of paper.<sup>67</sup> In general, when selecting the ideal paper substrate for PADs' applications, it is essential to consider key factors such as thickness, weight, porosity, filtration speed, particle retention, wicking speed, and brightness.<sup>4</sup> The industry standard often favors thin papers, typically under  $100\text{ gm}^{-2}$ ,<sup>70</sup> due to their lower resistance to sample flow, which facilitates faster flow rates, reduced reaction times, and accelerated analytical responses.<sup>102</sup> Furthermore, the thickness of the paper plays a pivotal role in influencing factors such as optical path length, light scattering, and the required sample volume for assays. Evans and coworkers<sup>103</sup> present that thicker substrates (grade 3 chromatography papers) display a higher resistance to the fluid flow, resulting in slower sample solution transfers and suboptimal color development, which can be unfavorable to analytical readings. In contrast, thinner paper substrate (grade 1 chromatography papers) is demonstrated to have rapid solutions transfers and better analytical performance, with maximized color intensity and uniformity.

Porosity of a paper can influence the capillary flow rate; an enhanced porosity leads to an accelerated flow, which is important in determining the wicking speed.<sup>104</sup> This speed is not just a measure of efficiency but also a determinant of the crucial contact time between the sample and the reagent. Such interactions are important in influencing the intensity and uniformity of color in colorimetric  $\mu$ PADs. Ensuring high-quality results depends on this precise control of wicking speed, which is, in turn, determined by the channel size within the paper substrate. It is noteworthy that a narrower channel width can significantly reduce the wicking speed, underscoring the importance of these parameters for the design and engineering in the development of these devices.<sup>105</sup> The natural compatibility of cellulose fibers with biomolecules makes paper based technology useful for a range of biosensing applications.<sup>73</sup> In summary, paper-based biosensing devices represent a cutting-edge solution for rapid and on-site detection of target analyte. PADs boast a range of benefits, including their straightforward design, single-use convenience, chemical compatibility, low sample usage and the inherent porosity facilitating fluid movement *via* capillary action, eliminating the necessity for external pumping mechanisms.<sup>10,73,98,106</sup>

The mentioned functionalities of PADs are substantially enhanced by the controlled integration of metal nanoparticles

(MNPs), using the MNP stabilization techniques discussed in the preceding section (Section 4). The current section will explore diverse paper-based device architectures and how they facilitate the application of MNPs for advanced analytical purposes. The evolution of PADs began with paper chromatography and dipstick assays for simple, rapid detection, often enhanced by MNPs for visual cues. These developed into Lateral Flow Assays (LFAs), which use capillary action and MNP-labeled markers for easy, fast, and low-cost single-analyte detection, though with limited fluid control. Advances led to paper-based microzone plates enabling multiple tests in small areas, with MNPs boosting signals but often at the cost of sensitivity and increased noise. The most advanced form,  $\mu$ PADs, combine paper's low cost and porosity with microfluidics to enable precise, pump-free fluid control *via* hydrophilic channels.  $\mu$ PADs support multiplexed, quantitative analysis using small samples and diverse detection methods (colorimetric, electrochemical, SERS) enhanced by MNPs. Meeting ASSURED criteria,  $\mu$ PADs offer a powerful, affordable solution for rapid, on-site diagnostics, especially in resource-limited settings. Given their superior functionality and diagnostic potential, this review primarily focuses on  $\mu$ PADs as the most promising class of paper-based analytical devices.

### 5.1 Dipstick assays

A dipstick assay is a type of diagnostic test used to detect the presence or absence of specific substances in a liquid sample, such as urine, blood, or other fluids.<sup>7</sup> It typically consists of a test strip (often cellulose paper) coated with a specific reagent and an optional plastic stick, as shown in Fig. 4a. When the strip is dipped into a sample, a chemical reaction occurs between the reagents and target analytes, producing a visual change (often a color change) that indicates whether the target substance is present or absent.

Dipstick assays are particularly valued for their ease of use and the speed at which results can be obtained, often within minutes. These assays are also cost-effective, as the materials and processes involved in their production are inexpensive, making them ideal for widespread use in routine diagnostics. Among various factors contributing to the functionality of dipstick assays, the incorporation of MNPs plays an important role by enabling visual detection through colorimetric responses to target analytes.<sup>107</sup> Despite being inexpensive and simple to use, dipsticks only support one-step procedures without providing quantitative information. Extended incubation times can intensify color development, potentially leading to false results; thus, precise timing is essential for achieving even semiquantitative accuracy. In addition, color interpretation is inherently subjective and may vary between users, introducing variability in test outcomes.

### 5.2 Lateral flow assays

Lateral flow assay (LFA) is based on antigen–antibody interactions and operate on the principle of capillary action, where a liquid sample, such as blood, urine, or saliva, moves along a strip, interacting with components embedded in the device to





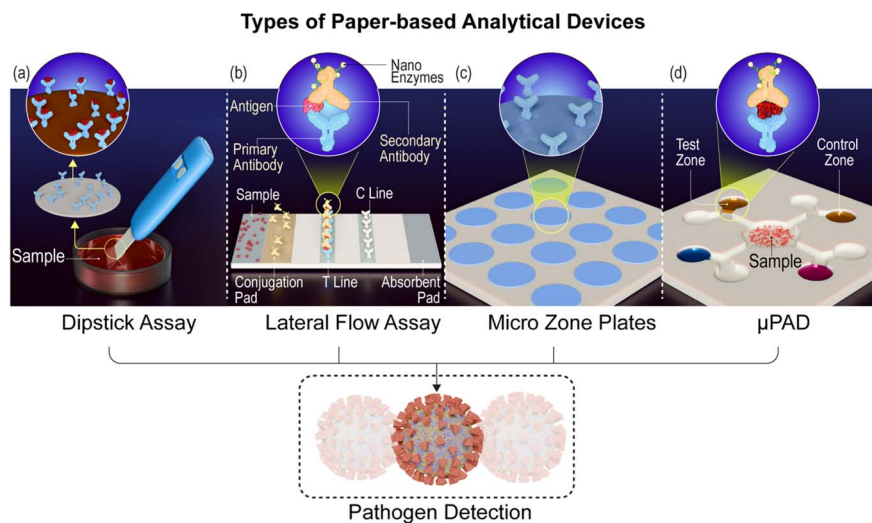


Fig. 4 Different types of paper-based analytical devices (a) dipstick assay, (b) lateral flow assay, (c) micro zone plates, and (d)  $\mu$ PAD.

produce a detectable signal (see Fig. 4b). LFA is mainly composed of a sample pad, a conjugated pad, a cellulose membrane, and an absorbent pad.<sup>3</sup> The liquid sample is mixed with a buffer before being applied to the sample pad.

The conjugate pad contains specific antibodies or molecules that are labeled with a detectable marker, such as metal nanoparticles or enzymes. In this context, MNPs (*e.g.*, AuNPs) serve as crucial detectable markers.<sup>108,109</sup> These are labeled with specific antibodies or molecules that bind to target analytes and generate a visible signal, typically a colored line, enabling optical or colorimetric detection within the LFA. As the sample flows across the nitrocellulose membrane, the target substance is captured by immobilized antibodies on the test line, generating a visible signal, often in the form of a colored line. A control line (C-line) ensures the test worked properly by capturing any remaining detection reagents, regardless of whether the target is present. Finally, the excessive sample reaches the absorbent pad. The absorbent pad is made of plant fiber or filter paper and prevents the liquid to flow reverse.

LFAs are primarily used for their ease of use, speed, affordability and ability to deliver rapid results without the need for complex instrumentation or extensive sample preparation. They are available for a range of applications, including hormone, pathogen, pesticide, and drug detection. However, LFAs have limitations. They generally offer low sensitivity and limited specificity, with challenges in achieving accurate quantitative or multiplexed results. Their repeatability can be inconsistent, and the lack of fluid control due to the absence of microchannels restricts assay complexity.<sup>8,109</sup>

### 5.3 Paper-based microzone plates

Paper-based microzone plates are a type of analytical device used for performing chemical or biochemical tests in small, well-defined areas on a piece of paper, Fig. 4c.<sup>9</sup> Compared to plastic plates, paper micro-zone plates benefit from advantages, such as low-cost, disposable, small volume requirement of

reagents/samples, and easy stacking and storage of the plates. Each microzone is typically pre-treated with specific reagents or chemicals that react with the sample applied to it, allowing for colorimetric or other types of detection methods. To enhance signal generation and improve sensitivity, MNPs can be integrated into these microzones. Their incorporation amplifies the optical readout, making paper-based platforms more powerful and effective for analytical applications.

The paper micro-zone plate can be designed in 6-, 12-, 24-, 96-, and 384- zones like plastic microwell plates, often printed or fabricated using techniques such as wax printing, inkjet printing, or laser cutting. These methods help to define the boundaries of each zone and ensure that the reactions take place in isolated areas without cross-contamination between different microzones. ELISA assay by paper micro-zone plate<sup>110,111</sup> is faster and the responses can be recorded by smartphone or scanner. Because paper-based microzone plates can be modified with different reagents, they are highly versatile and can be tailored to detect a wide range of substances, from pathogens to environmental contaminants. However, it is less sensitive and has higher background noise compared to traditional laboratory equipment, such as microplates used in ELISA (enzyme-linked immunosorbent assay) or PCR (polymerase chain reaction) techniques.

### 5.4 Microfluidic paper-based analytical devices ( $\mu$ PADs)

**5.4.1 Introduction to  $\mu$ PADs and fabrication methods.** Microfluidic paper-based analytical devices ( $\mu$ PADs) feature narrow hydrophilic channels within a porous paper matrix, bounded by barriers that confine the lateral flow of fluids as shown in Fig. 4d. These devices support a range of functionalities, including liquid transport, mixing, separation, and chemical reactions, all within a compact and efficient format. Various detection techniques, such as colorimetric, electrochemical, electrochemiluminescence *etc.*, have been integrated into  $\mu$ PADs, enabling highly sensitive analyte detection.<sup>19</sup> In this



section, we provide an overview of the fabrication methods developed for  $\mu$ PADs to date, along with their respective advantages and limitations. The fluid confining barriers are defined either by surface modification of paper using hydrophobic materials which block the cellulose nano-pores, or by mechanical creation of voids which physically separate the channels from the rest of the matrix. To achieve the impregnation of hydrophobic substances into the paper matrix, indirect or direct patterning methods are adopted. Indirect patterning refers to the use of an intermediate mask for the channel or barrier creation. Methods such as UV lithography, vapor phase deposition, plasma treatment, and screen printing utilize a mask or screen to transfer patterns onto the paper surface. In the direct patterning strategy, hydrophobic substances (inks) that form the barriers are printed directly onto the paper surface. This method often includes a post-heating step, allowing the substance to permeate into the porous matrix. Conventional printing techniques like wax printing, inkjet printing, flexographic printing, and laser toner printing are examples of direct patterning. Alternatively, techniques that employ physical separation of the paper channels through cutting with sharp objects or laser-assisted cutting have been employed for  $\mu$ PAD fabrication for faster and chemical-free process.

**5.4.2 Indirect patterning of hydrophobic barriers.** Martinez *et al.* demonstrated the first complete  $\mu$ PADs, with hydrophilic channels created by conventional photolithography, and used them for colorimetric detection of glucose and paper-based Elisa.<sup>100,111</sup> This method involved the wet chemical processing of chromatography paper with photo-active polymers and multiple baking steps. Photolithography guarantees the highest resolution of channel and barrier widths since they are created with high precision lithography equipment. However, the process is complex and not a low-cost, scalable solution for the production of  $\mu$ PADs. Vapor phase deposition of the hydrophobic reagents is a dry, substrate-independent, bottom-up method adopted to avoid the use of liquid reagents, resists and solvents. In this technique, monomers of hydrophobic

polymers along with initiators are evaporated and then converted to radicalized monomers by pyrolysis at high temperatures inside a vacuum reactor. The vapor phased monomers and free-radicals are deposited on the paper substrate with the aid of a mask. These chemical precursors adsorb and react on the paper surface, where they polymerize and form hydrophobic walls. Functional polymer films such as hydrophobic poly(1H,1H,2H,2H-perfluorodecyl acrylate), click-active poly(pentafluorophenyl methacrylate), and light-responsive poly(*ortho*-nitrobenzyl methacrylate) and poly(chloro-*p*-xylene) [PPX] were coated on paper substrate using this method.<sup>112,113</sup> Lam *et al.* demonstrated the chemical patterning of hydrophobic trichlorosilane (TCS) on paper by a chemical vapor deposition (CVD) method.<sup>114</sup> Vapor phase deposition stands out as a highly efficient technology to build single-step functional polymer-based circuits on paper, but it demands sophisticated vacuum-based instrumentation, costly reagents and pre-manufactured masks. Screen printing is another indirect patterning method for the fabrication of  $\mu$ PADs. Here, a hydrophobic ink (for *e.g.*, paraffin wax) is firmly rubbed and squeegeed-off over a custom-made stencil screen placed on the paper surface. The ink is then melted and impregnated into the paper matrix by heating (Fig. 5a). This turns the paper hydrophobic everywhere, except the masked regions. Several low-cost alternatives of wax such as polystyrene, poly (methyl methacrylate) (PMMA), polydimethylsiloxane (PDMS), polycaprolactone and polylactic acid have been found compatible for screen printing.<sup>115</sup>

**5.4.3 Direct patterning of hydrophobic barriers.** In wax printing process, molten wax is directly printed on the hydrophilic paper surface, using patterns designed in a computer. It involves two steps: the printing using a solid ink printer, followed by heating using a hotplate (Fig. 5b). The heating step enables the infusion of wax into the paper cross section, which creates hydrophobic walls of wax in the porous matrix.<sup>116</sup> This widely adopted direct patterning approach is limited by its poor resolution due to the lateral spreading of wax. Moreover, the discontinuation of commercial wax printers has made

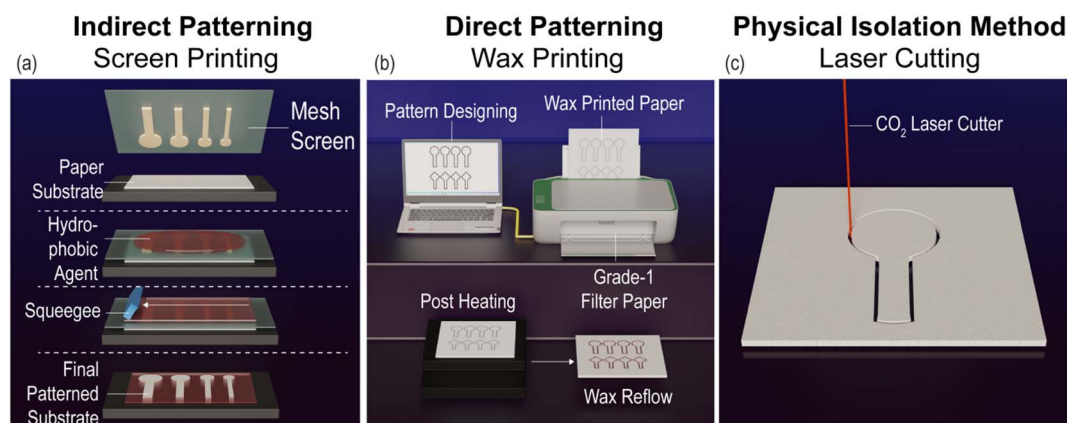


**Fig. 5** Representative fabrication techniques for  $\mu$ PADs. (a) Screen printing: patterns are first defined on a stencil screen and then transferred onto the paper substrate to create distinct hydrophilic and hydrophobic regions, (b) wax printing: hydrophobic wax is directly printed onto the paper using a commercial wax printer, which, upon heating, diffuses to form barriers, (c) laser cutting: grooves are precisely etched into the paper substrate using a laser cutter to physically define and isolate hydrophilic microchannels from the surrounding matrix.



researchers to look for alternate fabrication methods. Inkjet printing refers to the contactless spraying of ultra-tiny droplets of liquids onto a substrate.<sup>117,118</sup> This method has been employed to create bio-active surfaces for applications in chemistry and biology. The inkjet-principle is used for the fabrication of channels and barriers for  $\mu$ PADs. In a direct approach, the ink in the inkjet printer is substituted with a hydrophobic liquid, which is then dispensed over the hydrophilic paper.<sup>119</sup> In an alternative approach, the paper is fully hydrophobized using a hydrophobic polymer solution in the initial step. Then, an inkjet of a suitable solvent, is used to etch the hydrophobized surface, effectively restoring its hydrophilic properties.<sup>120</sup> Like the photolithography technique, the inkjet printing method also involves the complete treatment of paper with solvents, and other chemicals. The clogging of the printer nozzle, and comparatively slower printing process are some of the limitations of the inkjet printing. In a recently developed approach with laser toner printer, solid toner ink is used to create hydrophobic patterns on paper. It involves the automated printing of the design on paper and a post-baking step.<sup>121</sup>

**5.4.4 Physical separation of paper channels.** Paper cutting is one of the simplest and easiest technique to fabricate  $\mu$ PADs. The necessary hydrophilic channels are physically separated from the rest of the porous medium. The boundaries are defined by voids, and hence this method does not involve the use of reagents and solvents. The natural hydrophilic characteristics of the cellulose medium is preserved. Paper sheets can be manually or mechanically cut using a knife or scissors to create simple dipsticks and chromatographic devices. Laser-based cutting method is suitable to cut narrow, length or complex shapes of paper sheets (Fig. 5c). It offers the speed, precision, scalability, and automation required for mass production of  $\mu$ PADs. A high-power commercial laser such as CO<sub>2</sub> laser is used to ablate of the cellulose structure and cut through the paper matrix in a controlled manner.<sup>122</sup> Cutting of the paper sheets results in free-standing hydrophilic channels, which require a supporting platform for mechanical strength.

Recently, Kumawat *et al.* developed a hybrid method, where initially the laser-cut patterns are made in lamination sheets, which are then transferred to the paper sheet.<sup>123</sup> Here, filter paper sheet was sandwiched inside the precut lamination pouch and heated with a hotplate. The melted Ethylene-vinyl acetate (EVA) from lamination sheets impregnated to the porous medium to form the hydrophobic barrier. These devices have high mechanical strength against bending, folding, and tearing, and are resistant to strong acids, bases, and solvents. A comparative overview of various paper-based analytical devices, including their advantages and disadvantages, is summarized in Table 1.

**5.4.5 Plasmonic sensing mechanisms in  $\mu$ PADs Integrated with MNPs.** The integration of MNPs into the microfluidic paper-based analytical device represents a significant advancement in the development of rapid and highly sensitive diagnostic tools. While extensive literature exists on optical  $\mu$ PADs, the application of MNPs within this context is still an emerging area of research. The most used nanomaterials in paper-based devices are AuNPs for their remarkable labeling capabilities.<sup>124</sup> The inherent properties of AuNPs, such as their ease of functionalization, manipulability, biocompatibility, distinctive surface plasmon resonance, and electrochemical activity, render them exceptional for both optical and electrical detection applications.<sup>125</sup> However, the versatility of paper devices extends beyond AuNPs, incorporating a variety of other nanomaterials like magnetic nanoparticles,<sup>126</sup> quantum dots,<sup>127</sup> liposomes,<sup>128</sup> carbon nanoparticles<sup>129</sup> *etc.*

The integration of these NPs into  $\mu$ PADs paves the way for a multitude of detection mechanisms, including colorimetric, SERS-based methods, chemiluminescence, electrochemical, and electrochemiluminescence, which collectively ensure a robust and comprehensive sensing platform. In particular, plasmonic sensing mechanisms in  $\mu$ PADs that incorporate MNPs harness the unique optical characteristics of MNPs. These capabilities stem from their ability to concentrate electromagnetic fields at the nanoscale, especially through localized

**Table 1** Detection methods, advantages and disadvantages of different paper-based analytical devices

Type of paper-based device	Detection methods	Advantages	Disadvantages
Dipstick assays	• Optical	<ul style="list-style-type: none"> <li>• Ease of use</li> <li>• Rapid detection</li> <li>• Cost-effective</li> <li>• Easily disposable</li> </ul>	• No quantification
LFA	<ul style="list-style-type: none"> <li>• Optical</li> <li>• Electrochemical</li> </ul>	<ul style="list-style-type: none"> <li>• Possible quantification</li> <li>• Ease of use</li> <li>• Speed</li> <li>• Affordability</li> <li>• Multiplexed detection</li> <li>• Capillary flow</li> </ul>	<ul style="list-style-type: none"> <li>• Long detection times</li> <li>• Large sample volume</li> </ul>
Microzone plates	• Optical	<ul style="list-style-type: none"> <li>• Easily disposable</li> <li>• Low-cost</li> <li>• Rapid detection</li> </ul>	<ul style="list-style-type: none"> <li>• Less sensitive</li> <li>• High background noise</li> </ul>
$\mu$ PADs	<ul style="list-style-type: none"> <li>• Optical</li> <li>• Electrochemical</li> <li>• Luminescence</li> <li>• Chemiluminescence</li> <li>• MEMS</li> </ul>	<ul style="list-style-type: none"> <li>• Capillary flow</li> <li>• Quantification</li> <li>• Small sample volume</li> <li>• Industrial production</li> <li>• Different detection methods</li> </ul>	• Long detection times





surface plasmon resonance (LSPR). This phenomenon is foundational to two major biosensing approaches in  $\mu$ PADs: colorimetric sensing and SERS-based detection, both of which are instrumental in advancing the sensitivity and specificity of paper-based analytical devices.

**5.4.5.1 Colorimetric sensing.** Colorimetric sensing is one of the most widely used detection methods in  $\mu$ PADs, particularly when MNPs are integrated. This method leverages the unique optical properties of metallic NPs, which undergo visible color changes in response to specific analyte interactions. The fabricated hydrophobic/hydrophilic structure of the patterned paper prevents the uncontrolled spreading and dilution of the samples as well as of the chemical sensing inks. The easy read-out of the generated chemical signals and instrument-free measurements, makes this method an effective, simple, and cost-efficient tool for various analytical applications, such as disease diagnostics, environmental monitoring, and food safety.

Colorimetric detection often relies on the aggregation or disaggregation of NPs in response to a target analyte. The interaction between the analyte and surface-modified NPs induces a visible color change that can be easily detected by the naked eye, a smartphone camera or a handheld reader. In  $\mu$ PADs, multiple detection zones are crafted within a single device, each zone is designed to capture different analytes

through the strategic immobilization of highly selective biorecognition elements.<sup>130</sup> These elements (antibodies, oligonucleotides *etc.*), arranged in patterns such as lines or spots, interact with labeled samples *via* enzymatic or chemical reactions.<sup>131</sup> These interactions are enhanced by the use of cutting-edge plasmonic NP-decorated biorecognition probes. The synergy between flow control in paper-based microfluidics and the specificity of the biorecognition probes ensures that these zones act as focal points for biorecognition events. These events are marked by NPs, creating a visually detectable signal that clearly indicates the presence or absence of the target molecule. For example, early studies on colorimetric sensing in  $\mu$ PADs has been reported for the detection of pH, total protein, and glucose in clinically relevant concentration ranges for urine analysis.<sup>100,120</sup> Upon introduction of samples into the paper-based microfluidic assay, they are channeled into the reaction zones. This leads to a color change, which can be easily quantified to determine analyte levels using a calibration chart.

A colorimetric test has been developed for quickly measuring two Alzheimer's disease biomarkers, fetuin B and clusterin, in blood samples.<sup>132</sup> This test involves modifying specific antibodies with AuNPs and applying them to paper pads. When the targeted biomarkers are present, the flow of biofluid towards these modified antibodies leads to an accumulation of AuNP-antibody complexes in the test area, triggering a color change

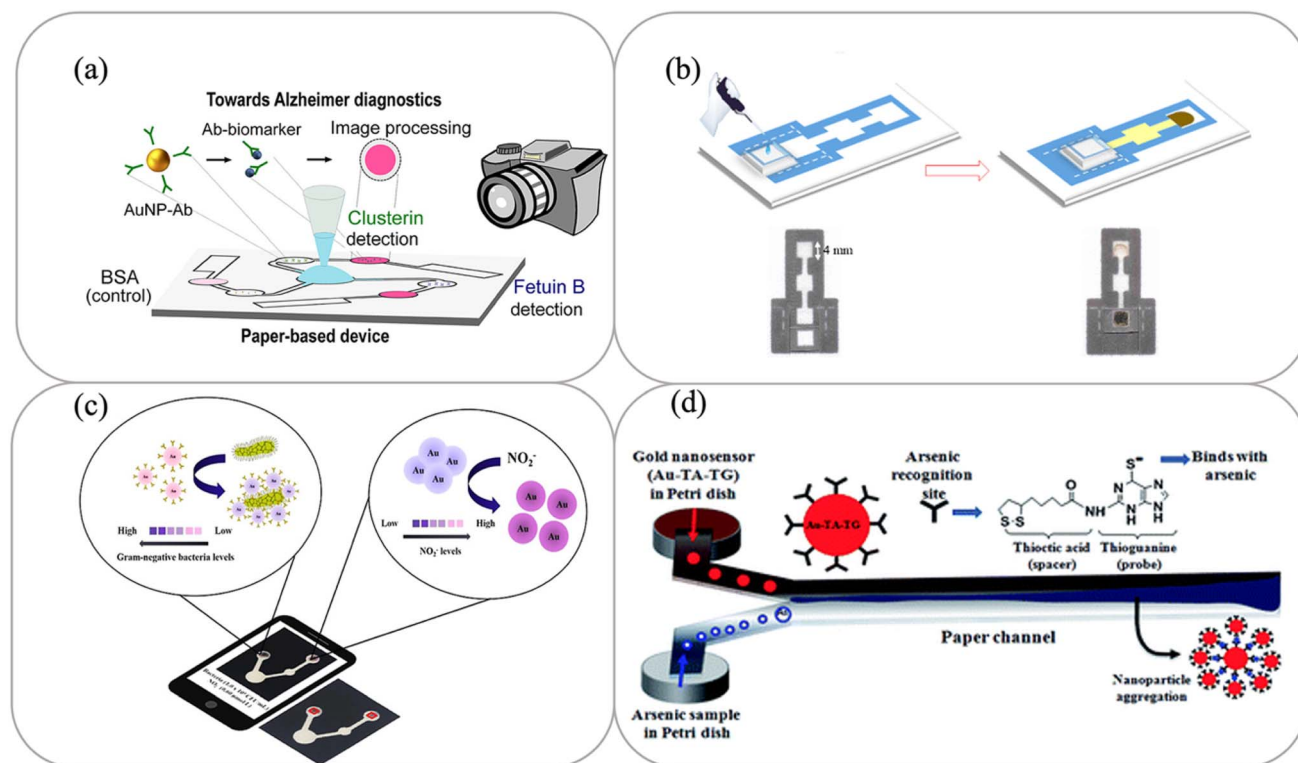


**Fig. 6** Different examples of colorimetric sensing mechanism in  $\mu$ PADs integrated with MNPs. (a) Detection of clusterin and fetuin B, by the modification of AuNPs in the presence of target analytes. This figure has been adapted from ref. 132 with permission from American Chemical Society, copyright 2019. (b) On-device formation of AgNPs through the interaction of uric acid. This figure has been adapted from ref. 133 with permission from SPRINGER NATURE, copyright 2018. (c) Detection of Gram-negative Bacteria and  $\text{NO}_2^-$  by the aggregation or antiaggregation of AuNPs. This figure has been adapted from ref. 134 with permission from American Chemical Society, copyright 2023. (d) Arsenic detection using gold nanosensor, Au-TA-TG. This figure has been adapted from ref. 135 with permission from RSC Publishing, copyright 2014.



from white to pink, as shown in Fig. 6a.  $\mu$ PADs have been reported that incorporates the visually striking plasmonic coloration produced through the *in situ* formation of MNPs. By utilizing specific analytes as reducing agents, salt precursors with noble metal complex ions are transformed into functional components. A prime example of this is the reduction of  $[\text{Ag}(\text{NH}_3)_2]^+$  by uric acid in the presence of NaOH, which results in the formation of AgNPs, thereby leading to a uric acid sensing platform,<sup>133</sup> Fig. 6b. The integration of AuNPs with a  $\mu$ PAD combined with a smartphone readout allowed for simultaneous monitoring of Gram-negative bacteria and  $\text{NO}_2^-$  levels in water and urine samples. AuNPs functionalized with polymyxin molecules (AuNPs@polymyxin) cause color change due to aggregation for the detection of Gram-negative bacteria, and de-aggregation in the presence of *o*-phenylenediamine (OPD) for  $\text{NO}_2^-$  detection,<sup>134</sup> (Fig. 6c).

Paper-based microfluidic aptasensors, combined with paper substrates, microfluidic channels and aptamers offer great potential for POC diagnosis, especially in resource-limited areas.<sup>136</sup> Aptamers, are known for their exceptional target binding affinities, robust stability, and ease of disposal compared to traditional probes like antibodies. These aptasensors facilitate the rapid and cost-effective detection of biomarkers, streamlining the diagnostic process to be both affordable and user-friendly.<sup>137</sup> Somvanshi *et al.*<sup>138</sup> demonstrated the design and development of microfluidic paper-based colorimetric multiplexed aptasensors. This includes the modification of AuNPs on polystyrene microparticles to create highly stable colorimetric labels. This results in an enhancement in signal sensitivity, due to an aggregation mechanism in the presence of target bacteria.<sup>138</sup>

$\mu$ PADs integrated with modified AuNPs can be used for the detection of mercury in air, fish and water samples.<sup>139</sup> The color of modified AuNPs in the test zone instantly changes after the addition of  $\text{Hg}(\text{II})$ , and this color change can be detected by the naked eye, or a digital camera.<sup>140</sup> A dual read-out colorimetric paper device integrated with MNPs was used for the evaluation of phenolic compounds by exploiting the growth of AuNPs and AgNPs.<sup>141</sup> Xie *et al.*<sup>142</sup> used a simple paper-based device for the SPR visualization of  $\text{Pb}^{2+}$  (one of the major environmental pollutants) with glutathione-modified AgNPs. A four-channel  $\mu$ PAD, comprising of AuNPs as colorimetric sensors and specific aptamers, is reported to simultaneously detect a wide variety of target analytes (that can detect mixtures of seized drugs) in a single device. The color change from the salt-induced aggregation of AuNPs indicates the presence of target analytes.<sup>143</sup> Nath *et al.*<sup>135</sup> demonstrated a simple, rapid and sensitive  $\mu$ PAD that can detect arsenic at very low concentration using a gold nano sensor utilizing the color change from the NP aggregation, Fig. 6d. Etching of AgNPs triggers a change in color from amber to grayish color. This can be judiciously employed as a visually observable sensing mechanism in food spoilage monitoring *via* paper-based devices incorporating MNPs; the release of ammonia from the food spoilage accompanied by other volatile organic compounds results in etching of AgNPs.<sup>144</sup> Other applications that utilize colorimetric sensing in  $\mu$ PADs

include biomedical testing,<sup>145</sup> environment monitoring<sup>146</sup> and food safety applications.<sup>134,147</sup>

One of the major disadvantages of colorimetric sensing in  $\mu$ PADs is its low sensitivity, making it difficult to detect low concentrations of analytes especially in complex samples. Additionally, visual interpretation of color changes can be subjective leading to inaccurate results.<sup>120</sup> Colorimetric sensors are also influenced by the background noise of the paper or the sample, especially problematic in biological samples like blood or urine. While colorimetric methods are excellent for qualitative or semi-quantitative analysis, accurate quantification typically requires the use of additional equipment (*e.g.*, smartphone cameras<sup>16,148–151</sup> or handheld readers<sup>102,152</sup>) to capture and analyze the color intensity. These limitations suggest that while colorimetric sensing is effective for many applications, especially in resource-limited settings, it may not be the best choice for high-precision or highly sensitive measurements.

**5.4.5.2 Surface-enhanced Raman scattering (SERS) sensing.** SERS is a powerful technique for enhancing the Raman signals of molecules, offering a highly sensitive platform for molecular detection. Paper-based substrates have garnered attention for SERS due to their cost-effectiveness, flexibility, and ease of use. This section outlines the basic principles of SERS detection, paper-based SERS substrates and the sensing mechanism in microfluidic paper-based SERS platforms.

**5.4.5.2.1 Background and mechanism.** Raman spectroscopy,<sup>153</sup> a vibrational spectroscopic technique based on Raman scattering, is a powerful tool for determining chemical species. Raman scattering is the phenomenon of inelastic scattering of photons from a molecule which is excited to higher vibrational energy levels.<sup>154,155</sup> The resulting spectrum reflects the energy differences between the incident and inelastically-scattered photons, giving the vibrational finger prints of a molecule.<sup>156</sup> However, the Raman signal is inherently weak (less than 0.001% of the source intensity), restricting the usefulness of this analytical tool.<sup>95</sup> Surface-enhanced Raman spectroscopy is a surface-sensitive technique that enhances the Raman signal by molecules that are adsorbed on metal nanostructured substrates (typically silver or gold).<sup>157</sup> This effect was first observed in 1974 by Fleischmann *et al.*,<sup>158</sup> while using Raman scattering to try to understand the electrochemical reactions of pyridine at a roughened silver electrode and this phenomenon was correctly interpreted in 1977.<sup>159,160</sup> The demonstration of single molecule detection using SERS was a strong stimulus for the field<sup>161</sup> and thereafter, with the rapid advancement in nanofabrication and Raman instrumentation, the huge potential of this technique is being fully exploited in numerous uni- and multidisciplinary approaches.<sup>162</sup>

The enhanced Raman signal in SERS arises from two primary mechanisms, first is electromagnetic (EM) field enhancement *via* localized surface plasmon resonances in metallic nanostructures<sup>163</sup> and the second is chemical enhancement (CE) due to charge transfer mechanisms.<sup>164</sup> The former arises from the interaction of light with plasmonic nanostructures, leading to enhanced local EM fields due to the resonant excitation of localized plasmon oscillations, which

amplify the EM field at the metal surface by  $10^2$ – $10^5$ -fold.<sup>91</sup> Molecules near this enhanced EM field experiences a stronger Raman scattering signal, contributing to a SERS signal enhancement in the range of  $10^3$ – $10^8$ -fold.<sup>165</sup> The strength of the EM field around NPs can be increased by tuning the morphology of nanostructures, dielectric functions and by interparticle plasmonic coupling thereby generating hotspots in the nanogaps of neighboring particles.<sup>166–168</sup> An illustration of SERS signal readout by employing plasmonic nanostructures is shown in Fig. 7. Besides EM enhancement, SERS can also be enhanced up to  $10^3$ -fold by CE, that can be attributed to the charge transfer between the adsorbed molecules and the metal surface,<sup>169,170</sup> although this mechanism is typically weaker than the EM contribution.<sup>171</sup> A detailed exploration of SERS mechanisms is beyond the scope of this article and can be found elsewhere.<sup>168,172,173</sup>

In the wake of remarkable strides in nanotechnology over recent decades, the applications of SERS have expanded into a myriad of new domains. These include environmental monitoring, medical diagnostics, art preservation, innovative textiles, and enhanced security measures.<sup>174–176</sup> The sensitivity and reproducibility of SERS measurements heavily depend on the nanostructured substrate. Research in recent years has focused on optimizing substrates to achieve uniform and highly reproducible enhancement.<sup>177,178</sup> Among the most significant advancements is the developments of nanoparticles arrays and nano assemblies particularly using AgNPs and AuNPs, which remain the most commonly used SERS substrates. When these NPs aggregates, they form a 3D distribution of hotspots, where the electromagnetic field is dramatically enhanced, leading to significant signal amplification.<sup>179–182</sup> These hot spots are crucial for achieving single-molecule detection. Another important development involves the synthesis of complex shaped nanostructures such as nanostars, nanoflowers *etc.* which offer improved enhancement efficiency due to their sharp features and high surface curvature. Fine control over the shape

and size of these nanostructures is essential for tuning LSPR and maximizing the enhancement effect.<sup>183,184</sup> Additionally, hybrid substrates that combine MNPs with other materials, such as graphene or metal oxides, have emerged as promising candidates for further improving both signal enhancement and substrate stability.<sup>185</sup>

Despite the successes of SERS, several challenges still remain. Reproducibility of SERS substrates is a critical issue, especially for quantitative analysis. The complicated substrate fabrication procedures make them inconvenient in common analysis. Advances in nanofabrication techniques<sup>186</sup> are expected to improve substrate reproducibility. The development of portable SERS devices enables on-site, real-time detection for applications such as environmental monitoring and point-of-care diagnostics.<sup>187</sup> Combining SERS with other technologies, such as paper microfluidics<sup>188</sup> have demonstrated to achieve new innovations in sensing and diagnostics, details of which are discussed in the below sections.

**5.4.5.2.2 Paper-based SERS substrate.** The surface on to which the NPs are placed can vary from rigid (*e.g.* glass, silicon wafers, hydrogels *etc.*)<sup>180</sup> to more versatile and flexible substrates (*e.g.* paper, cardboard substrates, plastic, commercial tape *etc.*).<sup>91,189,190</sup> Although traditional SERS substrates like silicon and glass, has very low SERS background signal, their limitations due to fragility and inflexibility, as well as the difficulty in the bonding procedures, can complicate the handling and collection efficiency of solid samples. The manufacturing costs and taxation processes associated with these materials prompted the shift to polymers, a versatile class of softer materials with diverse properties. Their gas permeability, optical transparency, and electrical insulation make them particularly useful in biological applications, especially in cellular assays. However, a significant drawback is that, due to their chemical composition and structure, polymers, such as PDMS, can exhibit Raman activity.<sup>191</sup> While flexible substrates

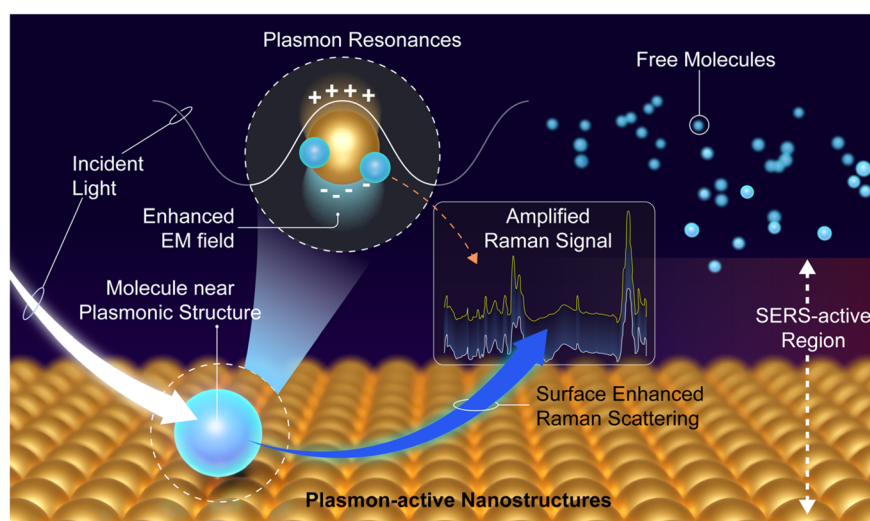


Fig. 7 Schematic depiction of the use of metal nanostructures to support LSPR for SERS enhancement, coupled with a dual strategy for achieving ultrasensitive SERS readout by combining analyte manipulation techniques with hotspot engineering.





like cellulose are not only less susceptible to damage but also offer the ability to conform to curved surfaces. This adaptability enhances the uptake and transport of analytes and maximizes the specific surface area, paving the way for groundbreaking advancements in bio-medical optical sensing.<sup>75,189,192,193</sup> Furthermore, paper-based SERS substrates can be integrated with existing analytical techniques, creating a cutting-edge platform that combines the strengths of conventional chromatography and microfluidics with biological assays, imparting chemical specificity to these techniques.

**5.4.5.2.3 Microfluidic paper-based SERS platforms.** The performance of a SERS-based microfluidic device is highly influenced by the material forming its structure. The selection of the material depends on the intended application, as each material offers distinct advantages and limitations (Fig. 8). Utilizing the individual strengths of paper-based microfluidics and SERS, several limitations inherent to both technologies can be addressed. Paper-based microfluidics excels in the precise control and manipulation of NPs within finely tuned channels, enabling significant advancements in the handling of micro-scale systems. This precision, coupled with the ability to work with minimal sample volumes due to its miniaturization capabilities, sets the stage for more efficient and cost-effective experimentation. The integration of SERS into paper-based microfluidic systems is not just complementary; it is essential. The robust detection capabilities of SERS are well suited to the small sensing areas and low sample volumes typical of microfluidic applications. The combination of these technologies has led to significant innovation. These platforms have demonstrated remarkable benefits and have been the focus of numerous impactful studies in recent years, which are highlighted in this section. In the previous sections, we have talked about the integration of MNPs in cellulose networks (section 4) and the patterning of hydrophilic channels in hydrophobic paper substrates (sub-section 5.4.1). These two methods will be used together to prepare microfluidic paper-based SERS platforms.

In a groundbreaking study, Li *et al.*<sup>194</sup> unveiled a revolutionary approach to fabricate AgNPs assays on the paper-microfluidic format for SERS detection that is both cost-effective and rapid. Their innovative spray-coating technique strategically deposits AgNPs onto paper substrates with channels created by wax printing, resulting in an array that significantly amplifies Raman signals. With a SERS enhancement factor of approximately  $2 \times 10^7$ , the fabrication process is also remarkably cost-efficient, with the total cost for 1000 chips falling below \$20. These compelling advantages underscore the promising future of the technique in expanding SERS applications across various fields such as environmental monitoring, and bioanalysis. Saha *et al.*<sup>195</sup> reported on the adaptation of using simple paper based microfluidic system where both the plasmonic nanomaterials and analyte are used in mobile phase, to facilitate controlled particle aggregation and the creation of electromagnetic hot spots within the microfluidic channels. The research highlights the use of Ag@Au NPs, approximately 25–30 nm in size, in conjunction with 4-mercaptopyridine as a Raman probe for the detection of streptavidin, Fig. 9a. The high sensitivity of the SERS response, recorded in a portable table-top Raman instrument, is from the NP aggregation which is triggered by the presence of proteins, creating electromagnetic hot spots. This approach has been successfully employed for the reproducible detection of proteins at concentrations ranging from picomolar to femtomolar levels. A paper membrane-based SERS system has been reported for identifying blood glucose levels, which used a nitrocellulose membrane as the paper substrate and a wax-printing process to create the microfluidic channel.<sup>196</sup> The rod-shaped gold nanorod particles were modified with 4-mercaptophenylboronic acid (4-MBA) and 1-decanethiol (1-DT) molecules and used as embedded SERS probe in this study, which is dropped into the hydrophilic channel of the membrane. Upon introduction of a blood sample into the hydrophilic channel, glucose molecules are efficiently transported to the SERS measurement area, retaining blood cells and proteins effectively on the membrane, streamlining the analysis. Microfluidics paper-based SERS platform has been employed for the on-site determination of

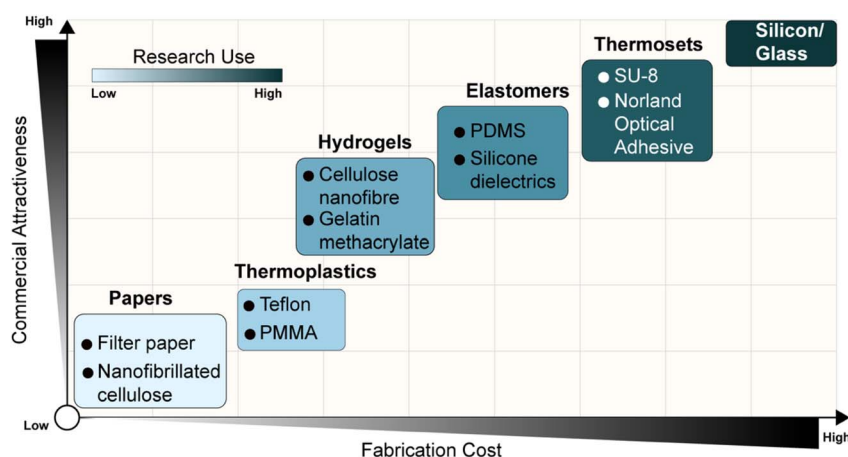


Fig. 8 The most promising materials for microfluidic chip fabrication and comparison of the resulting devices' cost.<sup>191</sup>

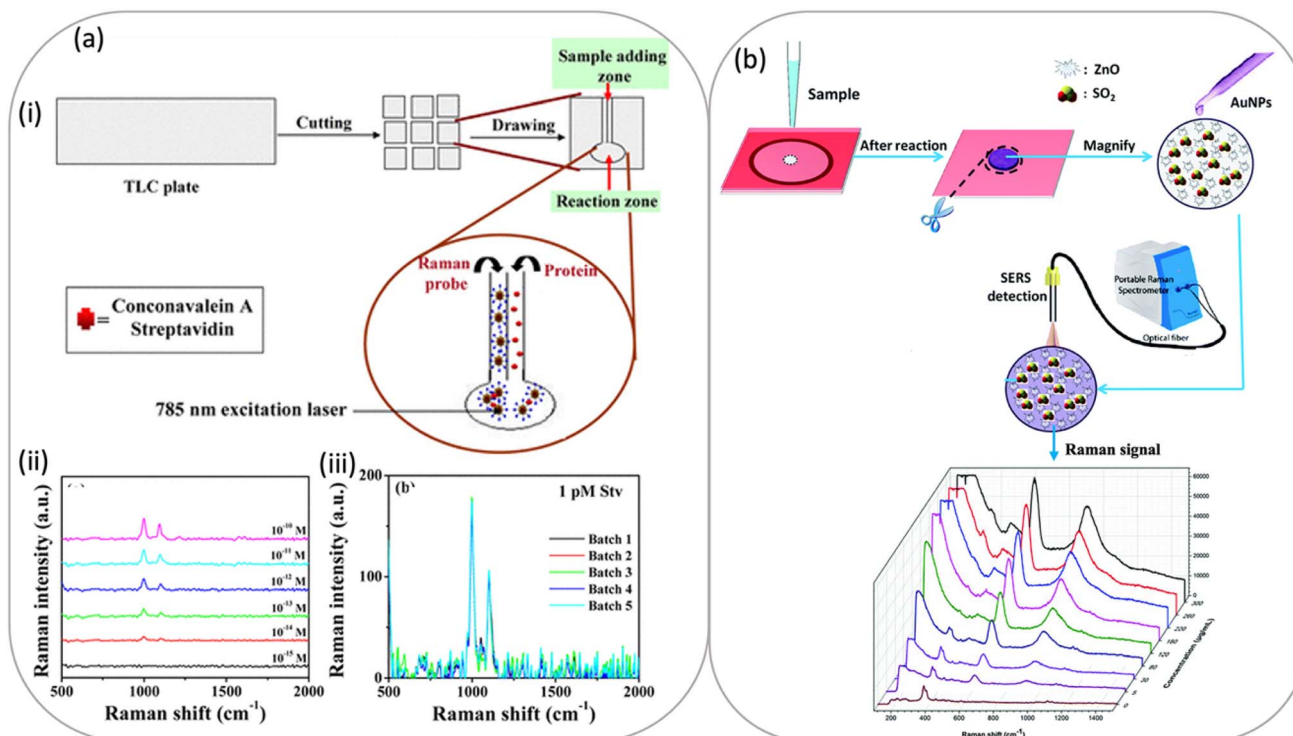


Fig. 9 (a-i) Fabrication of microfluidic chip from silica gel-based TLC (thin layer chromatography) plate, (a-ii) sensitivity and (a-iii) reproducibility of streptavidin detection in the microfluidic platform using biotin and 4-MPy-functionalized Ag@Au NPs. This figure has been adapted from ref. 195 with permission from American Chemical Society, copyright 2015. (b) Schematic illustration of  $\mu$ PAD-SERS for on-site detection of sulphite in wines. This figure has been adapted from ref. 197 with permission from RSC Publishing, copyright 2016.

sulphite in wine using a gas-diffusion method, Fig. 9b.<sup>197</sup> The SERS signal (detected through a portable Raman system) at a shift of 620 cm<sup>-1</sup> and SO<sub>2</sub> concentration demonstrated excellent linearity in the range of 5–300  $\mu$ g mL<sup>-1</sup> after extensive condition optimization.

As industrial technology has progressed, the production of numerous harmful substances has given rise to new environmental problems. Despite the implementation of various approaches to tackle these challenges, the results have been largely ineffective. A label-free, paper-based biosensing strip sensor with AuNPs was introduced to directly analyze the components of wastewater on site.<sup>198</sup> This SERS paper strip was fabricated by using wax printing and a successive ionic layer absorption and reaction (SILAR) technique (for AuNP deposition).<sup>199</sup> The biosensing performance of the fabricated SERS paper strip was evaluated by a standard Raman probe (*i.e.*, R6G) and confirmed with PABA (4-aminobenzoic acid) and pyrocatechol solutions and showed a sensitivity of 10<sup>-10</sup> M and an enhancement factor of  $2.8 \times 10^7$  for rhodamine 6G. The reported SERS-encoded paper strip offers potential benefits for on-site wastewater analysis. A few other research groups have as well employed  $\mu$ PAD-based SERS platforms for environmental monitoring and wastewater analyses.<sup>200,201</sup> Microfluidic paper-based SERS platforms are also reported to use in food safety applications.<sup>202,203</sup> For example, Zhu *et al.* used a  $\mu$ PAD (fabricated by cutting a hydrophilic region which had been printed on the filter paper and then pasting it onto sellotape) in the

determination of trace level of thiram in adulterated tea samples, Fig. 10a.<sup>204</sup> SERS probes were made of Au@Ag NPs with a 30 nm Au core and 7 nm Ag shell. The presence of thiram in sample solution is identified by the peak at 1143 cm<sup>-1</sup> because its intensity was highly sensitive in SERS experiments. A multifunctional platform for SERS-based POCT applications was reported, offering capabilities such as solid-liquid separation, small-molecule purification, and analyte collection through swabbing.<sup>205</sup> The composite SERS substrate, consisting of AgNPs and a filter membrane, is produced using a vacuum filtration method. Designed as a disposable sensing chip for POCT, the reported paper-based SERS chips demonstrated excellent sensitivity and repeatability when used with a smartphone-based Raman analyzer, Fig. 10b.

There are a few research works demonstrating the usage of  $\mu$ PAD-based SERS platforms for disease and health monitoring.<sup>206</sup> Teixeira *et al.* reported SERS-based paper nano sensors for ultrasensitive label-free detection of biomolecules in disease monitoring.<sup>207</sup> The paper SERS substrates were fabricated by assembling anisotropic particles, gold nanostars (GNSSs), and nanorods (NRs) onto paper to offer an extra enhancement to reach ultra-sensitive detection limits. Their preliminary results could distinguish different cell populations, which is of outmost relevance for the liquid biopsy field. Lim *et al.*<sup>208</sup> introduced a novel microfluidic SERS-based  $\mu$ PAD with multiple reaction zones designed for the simultaneous quantitative detection of various cardiac biomarkers—GPBB, CKMB, and



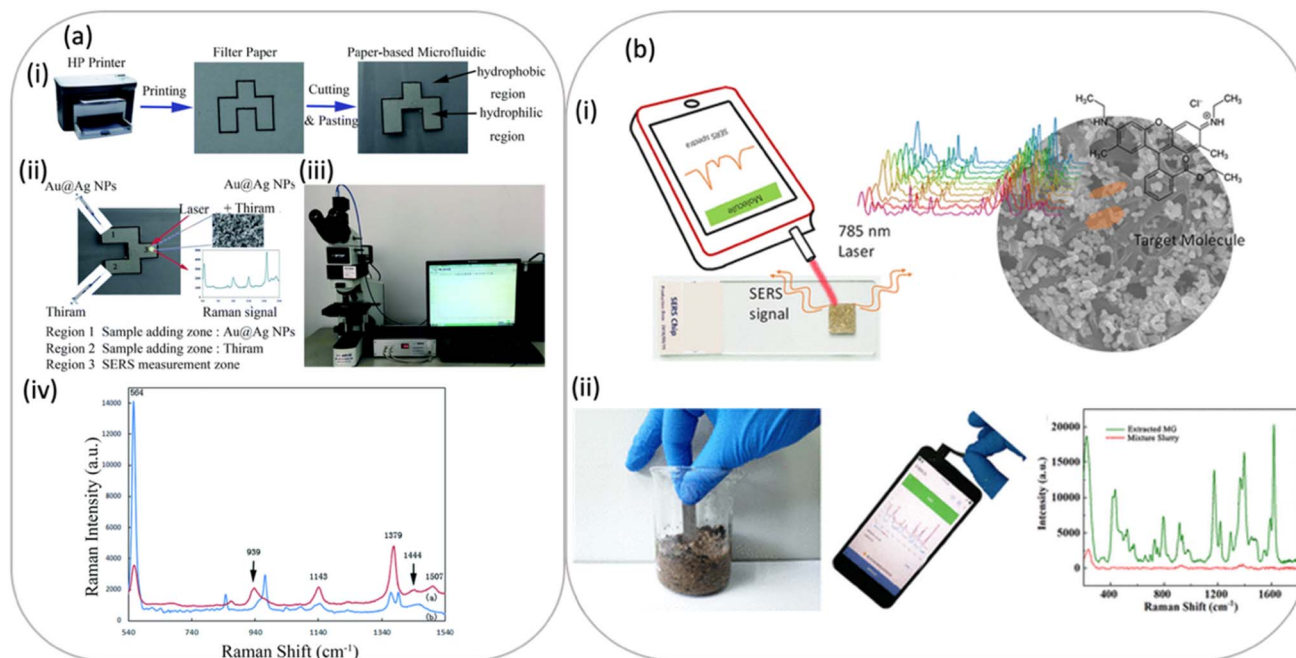


Fig. 10 (a-i) Fabrication process of the paper-based microfluidics, (a-ii) schematic of thiram assay procedure, (a-iii) schematic illustration of a micro-Raman spectrometer, (a-iv) comparison of SERS (with Au@Ag NP colloid) and normal Raman spectra of thiram powder. This figure has been adapted from ref. 204 with permission from RSC PUBLISHING, copyright 2017. (b-i) Scheme of the paper-based SERS chip with smartphone-based Raman analyzer (b-ii) photo showing the separation of MG from the mixture slurry of natural earth and MG by the SERS strip, Raman measurement on the SERS strip by the smartphone-based Raman analyzer, and SERS spectra of the extracted MG and the mixture slurry. This figure has been adapted from ref. 205 with permission from American Chemical Society, copyright 2019.

cTnT—for the early diagnosis and prognosis of acute myocardial infarction. They developed three distinct Raman probes, conjugated with specific antibodies, which were used as SERS nanotags to identify the cardiac biomarkers. This proof-of-concept technology shows great potential for the ultrasensitive, multiplexed quantitative identification of cardiac biomarkers in blood, potentially aiding physicians in making quicker and more informed decisions.

Mogera *et al.*<sup>209</sup> reported on wearable plasmonic sensors capable of detecting and measuring uric acid in sweat with high sensitivity, even at low concentrations of 1  $\mu$ M. The sensor system consists of multiple functional layers: a double-sided adhesive, a laser blocker, a paper-based microfluidic layer, plasmonic sensors, and a protective top layer. The microfluidic channel, crafted from cellulose chromatography paper in a serpentine design, efficiently moves sweat through its porous structure *via* wicking, eliminating the need for external pumps or pressure. Plasmonic sensors, strategically placed along this channel and crafted using a seed-mediated synthesis of gold nanorods (AuNRs), analyze sweat analyte concentrations at various times using Raman spectroscopy. This design incorporates a ratiometric SERS intensity method for analysis, which simplifies the process by removing the need for recalibration across different Raman spectrometers, thereby supporting widespread application of these sensors. The design of the sensor, being thin, soft, flexible, and stretchable, allows it to comfortably attach to the skin without causing irritation.

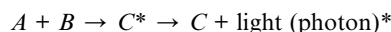
Paper microfluidic-based SERS devices offer significant benefits for a variety of analytical applications, yet there is a surprisingly small body of research dedicated to their development and documentation. This suggests that while the technology is highly promising, it is still in its early stages of exploration and adoption within the scientific community. Future research is essential to advance this field, expand its applications, and fully realize its potential benefits in analytical sciences.

**5.4.6 Non-plasmonic sensing mechanisms in  $\mu$ PADs integrated with MNPs.** This section focuses on the detection methods that employ the crucial non-plasmonic properties of MNPs within microfluidic paper-based analytical devices. Beyond their optical attributes, MNPs possess characteristics such as a high surface area to volume ratio, significant catalytic properties (especially in smaller NPs), and remarkable electronic conductivity. This section details how these non-plasmonic attributes enable MNPs to function as powerful tools in various sensing technologies, enhancing the capabilities of paper-based devices. Specifically, it explores their application in chemiluminescence, electrochemical, and electrochemiluminescence detection platforms, where MNPs can improve conductivity, increase surface area, introduce functional chemical groups, or act as catalysts to amplify signals. This comprehensive discussion aims to highlight the versatility of MNP-integrated  $\mu$ PADs for diverse analytical and diagnostic applications.





**5.4.6.1 Chemiluminescence sensing.** Chemiluminescence (CL) refers to the phenomenon where ground-state molecules absorb chemical energy from specific reactions, transition to an excited state, and subsequently emit light as they return to stability. At the molecular level, chemiluminescence involves the interaction of two or more chemical species—commonly referred to as reagents *A* and *B*—which undergo an exothermic reaction. This reaction yields an intermediate product, *C*<sup>\*</sup>, as the high-energy intermediate relaxes to its ground state, the excess energy is released in the form of visible light:



The CL detection method determines the concentration of the substance to be tested by measuring their emitted luminous intensity. The intensity and wavelength of the emitted light can be tailored by modifying the chemical structure of the reactants, enabling the development of highly specific and tunable detection systems. In recent years, the integration of MNPs such as AgNPs, and AuNPs has significantly broadened the scope for the sensing applications because of improved specificity and sensitivity.<sup>210–212</sup> The role of MNPs to a CL system is through various mechanisms such as surface plasmon coupling,<sup>212,213</sup> catalytic enhancement,<sup>212,213</sup> physiochemical properties because of high surface to volume ratio, and electron transfer

mediation.<sup>212,214</sup> Building on these advancements, researchers have applied the principles of CL enhancement through MNPs to develop innovative paper-based analytical devices. These platforms combine the high sensitivity and tunability of CL systems with the advantages of paper-based formats, enabling practical applications in POC diagnostics and environmental monitoring. Following are some examples of  $\mu$ PADs integrated with CL systems.

A laminated paper analytical device (LPAD) integrated with AuNPs was used for the detection of L-cysteine (L-cys) through CL.<sup>211</sup> This approach marked the first instance of employing the luminol and H<sub>2</sub>O<sub>2</sub> system in conjunction with AuNPs, revealing that L-cys could effectively inhibit the CL signal. By coating the paper surface with AuNPs, a significant enhancement in the sensitivity of L-cys detection was demonstrated. Based on this, a LPAD based on the inhibit effect of L-cys on the luminol–H<sub>2</sub>O<sub>2</sub>–AuNPs CL system was established to detect L-cys sensitively and cost-effectively. Liu *et al.* reported a wax-printed paper-based analytical device with AgNPs catalyzed luminol CL system for the determination of ofloxacin (OFLX) in eyedrop samples.<sup>215</sup> It was based on the enhancement of CL intensity of luminol–H<sub>2</sub>O<sub>2</sub>–OFLX system by AgNPs (Fig. 11a). This method can be useful for POC and environmental testing in remote regions and developing countries.

Another way of amplifying CL signal is by immobilizing more CL reagents by using nanoporous gold or silver (NPG or NPS).

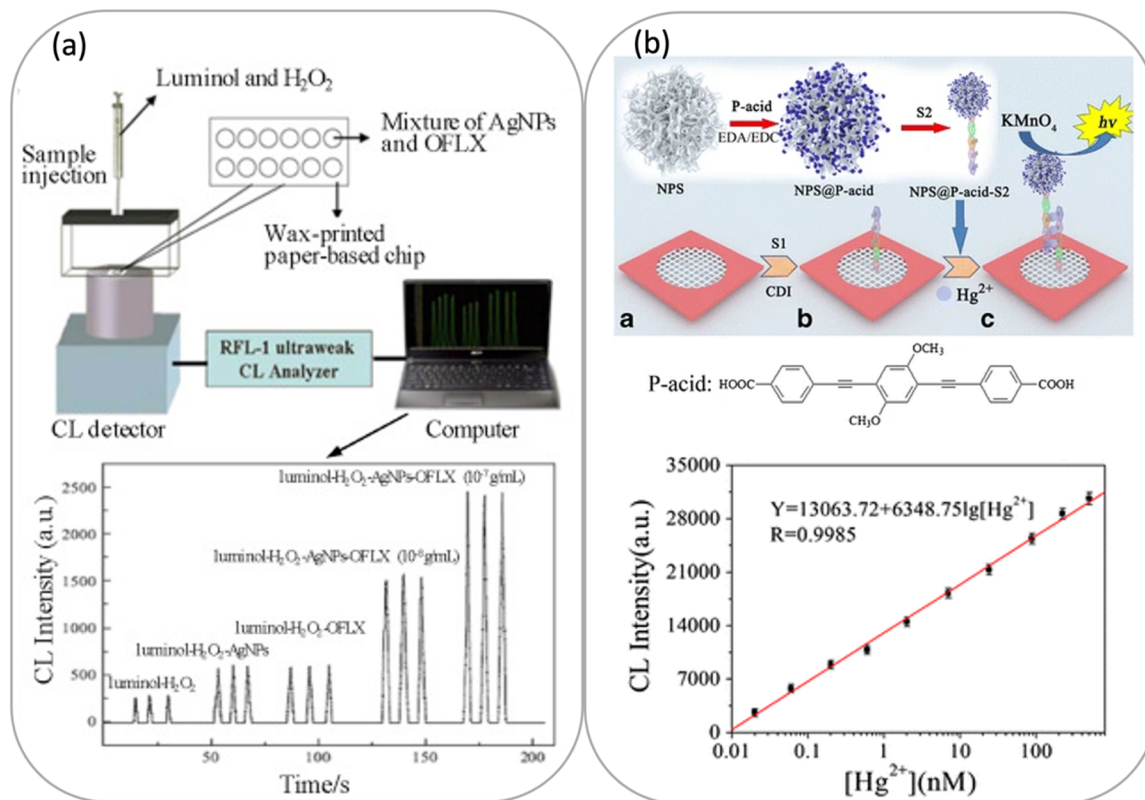


Fig. 11 (a) Schematic illustration and assay procedure of paper-based CL device for OFLX concentration determination. This figure has been adapted from ref. 215 with permission from Elsevier, copyright 2015. (b) Schematic illustration of fabrication process for paper-based CL device and calibration curve for Hg<sup>2+</sup> determination. This figure has been adapted from ref. 216 with permission from Springer Nature, copyright 2014.



This approach not only maximizes the surface to volume ratio but also ensures stability and bio-compatibility, crucial for sensitive applications. A novel CL aptasensor is designed to realize the simple and on-site determination of heavy metal ions in real samples, by incorporating the aptamer recognition elements onto  $\mu$ PADs.<sup>216</sup> The CL reagent (a caboxylated phenylene-ethynylene referred to as P-acid) was immobilized on NPS (NPS@P-acid) and used a CL label for the aptamer. A single-stranded DNA aptamer was first covalently attached to cellulose paper, utilizing the amino groups of the aptamer and the hydroxy groups on the paper's surface. The aptamer is capable of capturing Hg(II) ions through its specific interaction with thymine. The intensity of the CL signal is proportional to the concentration of Hg(II), as the presence of Hg(II) increases the amount of P-acid-conjugated aptamer, as seen in Fig. 11b. In another work, C-dots@NPG were used as the signal amplification label to obtain an ultrasensitive CL DNA biosensor by combining the amplification effect of the NPG and the CL performance of C-dots (carbon dots).<sup>217</sup> The developed  $\mu$ PAD biosensor (made by a rapid wax-screen-printing method), can be employed for the determination of trace amounts of analyte in real biological samples.

In their research, Li *et al.*<sup>218</sup> used a simple 3D  $\mu$ PAD with temporally resolved CL emissions to simultaneously detect three AMI biomarkers (H-FABP, cTnI and copeptin) in one CL detection. Sandwich-type CL immunoassays were constructed at different detection zones of the paper device by using Ab<sub>1</sub>-AuNPs immobilized on the  $\mu$ PAD as amplified capture probes and Co(II)-Ab<sub>2</sub>-luminol-AuNPs with excellent CL activity as novel amplified signal probes. This multiplexed immunodevice with a highly enhanced sensitivity have great potential in clinical application and point-of-care testing.

Chemiluminescence underlies many naturally occurring systems. In biology, it is the basis of bioluminescence which is observed in organisms such as fireflies and deep-sea creatures, where specialized enzymes catalyze reactions to produce light for communication, predation, or camouflage.<sup>212,219</sup> In analytical science, CL has become an indispensable tool in biosensing, immunoassays, forensic analysis, and environmental monitoring due to its high sensitivity, low background noise, and the ability to detect minute quantities of analytes.<sup>212,220</sup> However, these measurements must be conducted in the dark, which adds complexity to the manufacturing process of the device. Furthermore, this approach requires the use of a portable chemiluminescence reader. In addition to these practical challenges, many CL reagents lack high selectivity and can react with multiple analytes, leading to non-specific light emission that compromises measurement accuracy. Detecting trace amounts of substances is also difficult due to the inherently low intensity of the emitted light.

**5.4.6.2 Electrochemical sensing.** Electrochemical sensing is an analytical technique that translates biological interactions, typically between a target analyte and a biorecognition element, into quantifiable electrical signals, such as current, potential, conductivity, or impedance.<sup>221</sup> Owing to their high sensitivity, rapid response time, cost-effectiveness, and ease of miniaturization, they are particularly well-suited for POC diagnostics and

use in resource-limited environments.<sup>222,223</sup> Soon after its introduction, this relatively new adaptation of  $\mu$ PADs, known as electrochemical paper-based analytical devices (ePADs), quickly gained popularity within the POC research community.<sup>224</sup> This is largely due to the combined benefits of electrochemical sensing and the use of paper as an ideal substrate for POC testing platforms.<sup>225</sup> Traditional electrochemical systems on  $\mu$ PADs typically feature a three-electrode setup, consisting of a working electrode, a counter electrode, and a reference electrode.

The performance of an electrochemical device is primarily influenced by the shape, material composition, and fabrication techniques of its electrodes. Screen printing is currently the most common method for fabricating these electrodes on a paper substrate.<sup>224</sup>

One method to enhance the electrochemical properties of paper-based printed electrodes involves the deposition of MNPs, either by drop-casting, or by electro deposition or ink-printing. MNPs play a pivotal role in enhancing electrochemical functionality due to their unique physicochemical properties,<sup>226,227</sup> that may result in improved redox reaction kinetics, increased signal sensitivity, and reduced limitations related to commercial scalability.<sup>228</sup> The size, shape, and structural morphology of MNPs are especially critical in influencing their electrocatalytic activity, biomolecular binding selectivity, and interfacial interactions with electrodes or support materials.<sup>229–231</sup> Moreover, MNPs serve as anchoring sites for the immobilization of various recognition elements, such as DNA, aptamers, and antibodies.<sup>232</sup> The strategic modification of electrodes with MNPs not only enhances the electrochemical properties of paper-based devices but also directly translates into improved sensor performance, as demonstrated by various  $\mu$ PAD configurations employing different MNP types and deposition methods.

Nantaphol *et al.*<sup>233</sup> developed a  $\mu$ PAD for cholesterol detection, utilizing a boron-doped diamond (BDD) working electrode modified with AgNPs. The unmodified BDD electrode exhibited low sensitivity to H<sub>2</sub>O<sub>2</sub>, but the incorporation of AgNPs significantly enhanced the electrocatalytic activity for H<sub>2</sub>O<sub>2</sub> reduction, Fig. 12a. A recent study revealed that the carbon electrode in ePADs can effectively modify AuNPs, enabling the construction of electrochemically thiolated DNA probes.<sup>234</sup> It can also significantly boost both anodic and cathodic currents, as indicated by improved charge transfer, conductivity, and surface charge area compared to the paper electrodes (PE) without AuNPs (see Fig. 12b(I) and (II)). Such ePADs demonstrated high sensitivity in detecting microRNA 155, with a limit of detection (LOD) of 33.8 nM. Cinti *et al.*<sup>235</sup> produced paper-based electrochemical strips by applying AuNPs to a carbon electrode using a drop-casting method, targeting the detection of both single- and double-stranded DNA. AuNPs were also applied to graphene-treated cellulose fibers to improve the accuracy and stability of the system for DNA detection.<sup>236</sup> On commercially available screen-printed carbon electrodes, platinum NPs were electrodeposited, which enhanced the current response by catalyzing the oxidation of hydrogen peroxide at the electrode surface. Additionally, gold clusters were formed on the working



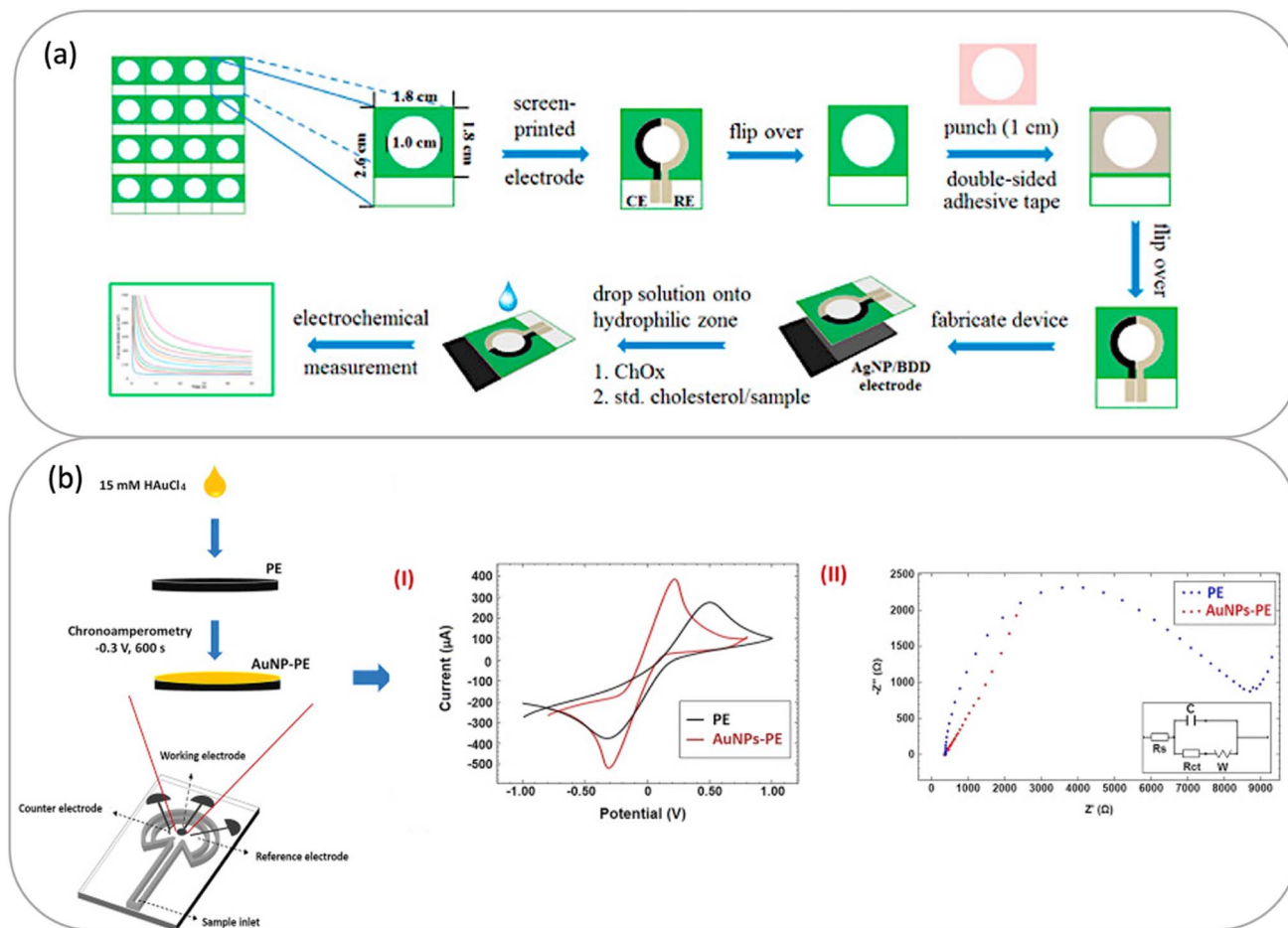


Fig. 12 (a) Schematic representation of the fabrication and analytical procedure for the cholesterol sensor based on the coupling of the AgNP/BDD electrode with  $\mu$ PAD. This figure has been adapted from ref. 233 with permission from Elsevier, copyright 2015. (b) Sketch of the AuNPs modified paper electrode sensing system, (i) CVs of PE and AuNP-PE, (ii) Nyquist diagrams of PE and AuNP-PE. This figure has been adapted from ref. 234 with permission from Elsevier, copyright 2021.

electrode through electrodeposition. Leveraging gold-thiol chemistry, the gold increased the surface area of the electrode and enabled the attachment of capture aptamers.<sup>237</sup>

Metal NPs have been innovatively used in the form of paper working electrodes (PWEs). These PWEs are created by developing interconnected layers of MNPs on the surfaces of cellulose fibers located in hydrophilic areas next to the printed electrodes. This manufacturing technique results in electrodes that are highly conductive and have a large surface area. Nanoporous silver (NPS),<sup>238</sup> platinum NPs,<sup>239</sup> etc. represents some of the PWEs that have been investigated for use in ePADs.

In general, electrochemical detection is an attractive sensing technique in  $\mu$ PAD technology due to their compact design, ease of portability, cost-effectiveness, high sensitivity, and exceptional selectivity. A notable feature of ePADs is their robust performance irrespective of lighting conditions, ensuring reliable results free from environmental interferences. One of the primary complexities of ePADs is the need to modify the electrodes. This process involves the complex construction of electrode systems on paper substrates and the precise printing of modification materials onto the electrode surfaces. Despite

these complexities, the versatility of ePADs is unmatched. They have the capability to utilize targets as both reactants to amplify electrochemical reactions and as impedances to attenuate them. This dual functionality makes ePADs an invaluable tool for detecting a diverse array of substances, including biomolecules, metals, and ions.

**5.4.6.3 Electrochemiluminescence sensing.** Electrochemiluminescence (ECL) is characterized by its ability to generate light through an exergonic electron-transfer reaction, initiated at the electrode surface, leading to the formation of excited states. It is the product of the combination of chemiluminescence and electrochemical methods that boasts reduced background noise and enhanced control over both the emission site and timing of the reaction.<sup>240</sup> In practical applications, ECL utilizes specific reagents and a co-reactant that, when electrified, produce a targeted light emission. This technology is particularly adept in the realm of  $\mu$ PAD-based detection, where it employs a sandwich immune structure. Here, a primary antibody is immobilized on paper-based substrates to capture the target analyte, while the ECL reagent is conjugated to a secondary antibody, serving as a precise and efficient label.





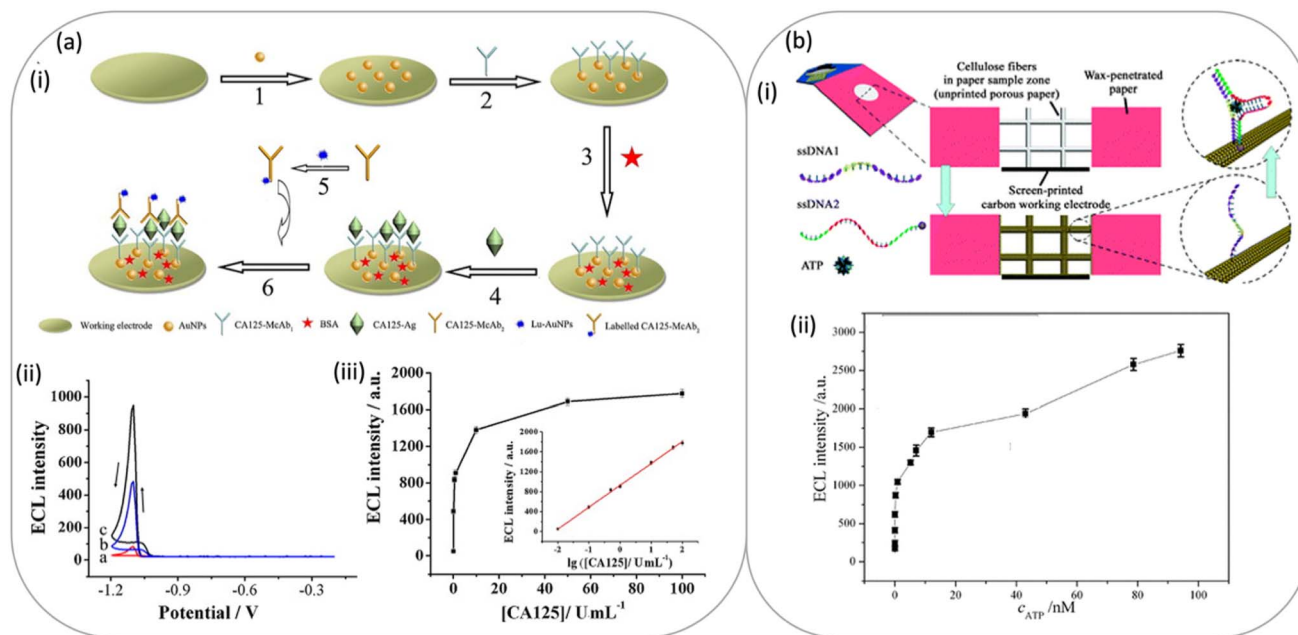


Fig. 13 (a-i) Schematic representation of the fabrication of the ECL immunosensor and assay procedure, (a-ii) ECL behaviors of the Lu-AuNPs labeled signal McAb<sub>2</sub> (curve a: 0.01 U mL<sup>-1</sup>, curve b: 0.1 U mL<sup>-1</sup> and curve c: 1 U mL<sup>-1</sup>), (a-iii) the calibration curve. This figure has been adapted from ref. 246 with permission from Elsevier, copyright 2013. (b-i) Schematic representation of the  $\mu$ -OECD for AT, (b-ii) relationship between ECL intensity and ATP concentration. This figure has been adapted from ref. 247 with permission from RSC Publishing, copyright 2013.

This synergy of precision and control positions ECL as a superior choice for analytical applications demanding high sensitivity and specificity.

In recent years, nanoparticles have been extensively explored for their ability to improve the performance of ECL-based detection method. A prevailing trend involves the synergistic integration of multiple nanoparticles, where the complementary properties of different nanostructures are combined to produce hybrid systems with superior electrochemical and luminescent characteristics.<sup>241</sup> MNPs, such as AuNPs and AgNPs, have emerged as key enhancers in ECL biosensors due to their exceptional electronic, catalytic, and surface properties.<sup>242</sup> Their incorporation into ECL systems has significantly improved sensitivity, signal amplification, and stability, making them ideal for ultrasensitive biosensing applications.<sup>243</sup>

In parallel with these advancements in MNP-enhanced ECL systems, considerable effort has been directed toward their integration with  $\mu$ PADs through the use of screen-printed electrodes on paper substrates, expanding the range of detection methods available for  $\mu$ PADs, for example, in the detection of immunoassays, biomarkers, biomolecules and drugs.<sup>244</sup> To further enhance the performance of ECL-based  $\mu$ PAD devices, attention has been focused on approaches that can improve the immobilization of bio-recognition substance in paper as well as the signal amplification for paper-based assays, majorly by the use of MNPs.<sup>245</sup>

In a work by Wang *et al.*,<sup>246</sup> luminol functionalized AuNPs (Lu-AuNPs) have been used as an ideal material for labeling and for signal amplification. By combining wax patterned 3D microfluidic origami device and screen-printed electrodes,

a sandwich-type ECL immunosensor was designed for determination of carcinoma antigen 125 (CA125). AuNPs were used as immobilization platform to improve electron transfer and enhance the immobilized amount of capture antibody (McAb<sub>1</sub>). Lu-AuNPs were synthesized as signal amplification section to label signal antibody (McAb<sub>2</sub>), Fig. 13a.

A porous Au-PWE was developed on a compatibly designed microfluidic origami ECL device ( $\mu$ -OECLD) through the growth of an interconnected AuNP layer on the surfaces of cellulose fibers in the paper sample zone.<sup>247</sup> This enhances the effective surface area of the working electrode for immobilizing the aptamer thereby increasing the sensitivity. The developed  $\mu$ -OECLD with dual amplification effects from Au-PWE and phenylene ethynylene derivative (P-acid) modified nanotubular mesoporous Pt-Ag alloy NPs (P-acid-Pt-Ag ANPs) can be easily integrated with other receptors such as antibodies for specific recognition of small molecules, like ATP (adenosine triphosphate) and proteins (Fig. 13b). In another work by Wu *et al.*<sup>248</sup> Au PWE was employed together with porous Au Pd alloy NPs as ECL nano labels to accelerate the ECL reaction in a microfluidic origami ECL device. The developed device displayed a low detection limit and wide linear range for quantification of cancer cells with desirable reproducibility and stability. Yan *et al.*<sup>245</sup> took the advantages of AuNPs and Graphene and the amplification effects of the Pt-Ag alloy NPs coupled with P-acid as well as the specificity of immunosensor and designed a microfluidic origami ECL immunosensor that has a low detection limit of 0.3 pg mL<sup>-1</sup>. The proposed method was applied to the determination of carcinoembryonic antigen (CEA) in samples with satisfactory results. One of the most



common ECL reagents used in  $\mu$ PADs is the inorganic complexes tris(2,2'-bipyridyl) ruthenium(II) ( $\text{Ru}(\text{bpy})_3^{2+}$ ) due to its advantages in chemical stability, reversible electrochemical behavior, and luminescence efficiency over a wide range of buffer pH levels. To enhance the luminous intensity of the  $\text{Ru}(\text{bpy})_3^{2+}$ -based ECL system, MNPs are integrated with it. For example, a  $\mu$ PAD has been proposed for simultaneous ECL detection of lead ion ( $\text{Pb}^{2+}$ ) and mercury ion ( $\text{Hg}^{2+}$ ) using the ECL nanoprobe ( $\text{Si}@\text{CNCs}$  and  $\text{Ru}@\text{AuNPs}$ ) based on a potential-control technique, in environmental monitoring and

medical diagnosis.<sup>249</sup> Recently Gao *et al.* synthesized Au nanocages that can adsorb  $\text{Ru}(\text{bpy})_3^{2+}$  as an ECL signal amplification label in a  $\mu$ PAD-based immunoassay, for ultrasensitive monitoring of CEA.<sup>250</sup>

ECL-based detection enhanced with MNPs in  $\mu$ PADs retains several key advantages such as high sensitivity, wide linear range, convenient observation, and simple instrumentation. Since the excitation in ECL is electrochemical rather than optical, the background signal is significantly reduced, leading to a high signal-to-noise ratio and improved detection

**Table 2**  $\mu$ PADS integrated with MNPs in colorimetric, electrochemical, chemiluminescence, electrochemiluminescence and SERS-based design

Mechanism	Type of nanoparticles	Target analyte	Applications	Ref.
Colorimetric	AuNPs	Fetuin B and clusterin	Early-stage diagnosis of Alzheimer's disease	132
Colorimetric	AuNPs decorated PS microparticles	<i>E. coli</i> and <i>S. Typhimurium</i>	Screening of pathogenic bacteria in water	138
Colorimetric	AuNPs	$\text{Hg}(\text{II})$	Food quality control	140
Colorimetric	AuNPs and AgNPs	Polyphenols	Total polyphenols content (TPC) analysis	141
Colorimetric	Glutathione-modified AgNPs	$\text{Pb}^{2+}$	Lake and river water quality monitoring	142
Colorimetric	AuNPs	Cocaine	Analysis of seized drugs	143
Colorimetric	AuNPs	$\text{As}^{3+}$ ions	Water quality monitoring	135
Colorimetric	AgNPs	Uric acid	Disease diagnosis	133
Colorimetric	AuNPs functionalized with polymyxin molecules	Gram-negative bacteria and $\text{NO}_2^-$ ions	Water quality monitoring	134
SERS	AgNPs	R6G		
SERS	Ag@Au NPs	Streptavidin	Point-of-care diagnostics	195
SERS	Au nanorod particles	Glucose in blood	Diabetes mellitus diagnosis	196
SERS	AuNPs	$\text{SO}_2$	On-site monitoring of sulphite in wine	197
SERS	AuNPs	4-Aminobenzoic acid and pyrocatechol	Point-of-assay of wastewater	198
SERS	Au@Ag NPs	Thiram	Food-safety	204
SERS	AgNPs-embedded nylon filter membrane (ANFM)	Crystal violet and malachite green	POCT analysis	205
SERS	Ag, Au-urchin and Au NPs	Cardiac biomarkers (GPBB, CK-MB, and cTnT)	Disease monitoring and early diagnosis	208
SERS	Au nanorods	Uric acid	Sweat analysis	209
CL	AuNPs	L-cysteine	Disease diagnosis	211
CL	AgNPs	Ofloxacin	Environmental testing	215
CL	Nanoporous silver (NPS@P-acid)	$\text{Hg}(\text{II})$	Biological and environmental monitoring	216
CL	Primary antibody functionalized AuNPs	AMI biomarkers	Early diagnosis of AMI	218
Electrochemical	AgNPs modified boron-doped diamond electrode	$\text{H}_2\text{O}_2$	Cholesterol detection	233
Electrochemical	AuNP-PE	miRNA	Early diagnosis of cancer	234
Electrochemical	Nanoporous gold-chitosan (NGC)	Carcinoembryonic antigen (CEA) and alpha-fetoprotein (AFP)	Blood protein analysis	238
Electrochemical	AuNP and PtNP functionalized CNT modified PES	$\text{Hg}^{2+}$	Public health and environmental protection	254
ECL	Luminol functionalized AuNPs	Carcinoma antigen 125	Determination of tumor markers	246
ECL	Porous AuPd alloy	MCF-7, HepG2 and SK-BR-3	Early diagnosis of cancer	248
ECL	$\text{Ru}@\text{AuNPs}$	$\text{Pb}^{2+}$ and $\text{Hg}^{2+}$	Environmental monitoring and medical diagnosis	249
ECL	$\text{Ru}(\text{bpy})_3^{2+}@\text{Au}$ nanocages	CEA	Analyte tracing in real biological samples	250



limits.<sup>251,252</sup> As a result, ECL-based detection exhibit excellent characteristics, including controllability, high sensitivity, and low background interference, making them particularly effective for applications in immunoassays, DNA hybridization detection, and clinical diagnostics.<sup>253</sup> It is important to note that, due to the reliance on ECL intensity for detection, certain protocols must be adhered to, such as safeguarding the detection environment from light and necessitating the labeling of the luminescent reagent, which introduces complexity to the reaction environment and material preparation.

A table summarizing the different sensing approaches employed in  $\mu$ PADs integrated with NPs is shown in Table 2.

## 6. Summary

The integration of nanomaterials, particularly metal nanoparticles (MNPs), with microfluidic paper-based analytical devices ( $\mu$ PADs) offers profound advancements for point-of-care (POC) diagnostic systems. This combination creates high-performance, portable, and user-friendly platforms that effectively meet the ASSURED criteria—affordable, sensitive, specific, user-friendly, rapid and robust, equipment-free, and deliverable to end-users. A key advantage of incorporating MNPs into  $\mu$ PADs is the substantial amplification of detection signals. This amplification is primarily due to the unique optical and physicochemical properties of MNPs, such as localized surface plasmon resonance (LSPR) and catalytic activity, which enable ultrasensitive analyte detection even at very low concentrations. These signal enhancements often result in visible colorimetric changes, facilitating equipment-free, naked-eye detection, which is particularly ideal for low-resource settings. Furthermore, MNPs offer exceptional multifunctionality, serving simultaneously as signal reporters, carriers of biorecognition elements (like antibodies, aptamers, or enzymes), and catalysts for amplification reactions. This versatility allows for the execution of more complex, multiplexed, or multi-step assays on a single paper device.

The current review has explored both the plasmonic and non-plasmonic attributes of MNPs in  $\mu$ PADs. Their plasmonic properties, such as LSPR, allow for light concentration and optical signal enhancement, while non-plasmonic features including high surface area, catalytic activity, and electronic conductivity, further elevate assay performance. Embedding these nanoparticles into the paper matrix, whether through solution-based methods or physical deposition techniques, significantly improves overall device sensitivity, response time, and durability. The physical structure of paper itself adds to this advantage. Paper is flexible, porous, and inexpensive, and it can be easily functionalized, making it an ideal substrate for POC diagnostics. The integration of MNPs into 2D and 3D  $\mu$ PAD architectures not only supports device miniaturization but also enables rapid assay execution. These features, combined with the compatibility of MNPs with scalable fabrication techniques, offer a clear path toward cost-effective and mass-producible diagnostic tools.

An important benefit of MNP integration is the customizability of the device response. By carefully tuning the size,

shape, and surface chemistry of MNPs, researchers can tailor the sensitivity and selectivity of the device, to detect a wide variety of targets, enabling label-free and real-time detection mechanisms. Importantly, many noble MNPs demonstrate biocompatibility and can readily interface with diverse biological recognition elements, making them suitable for detecting proteins, nucleic acids, pathogens, and small molecules in a variety of clinical and environmental applications.

By employing a diverse array of plasmonic nanostructures, several analytical approaches have been utilized, including colorimetric, SERS (Surface-Enhanced Raman Scattering) chemiluminescent (CL), electrochemical, and electrochemiluminescent (ECL) detection methods. Each approach offers unique strengths and limitations, and their integration into paper-based platforms broadens the scope of applications, ranging from disease diagnostics and food safety to environmental monitoring. Among all the detection techniques discussed in this review, microfluidic paper-based SERS platforms have gained significant interest due to their advantages, including low sample volume requirements, rapid analysis, cost-effectiveness, and time efficiency in detecting analytes. Recent advancements in Raman instrumentation, improved spectroscopic resolution, and the availability of specialized excitation wavelengths have addressed many previous limitations. Additionally, portable Raman systems enable on-site and real-time detection, making these technologies more accessible and practical.

## 7. Critical challenges and future perspectives

Despite the significant advantages of integrating metal nanoparticles (MNPs) into  $\mu$ PADs, several critical technical and translational challenges must be comprehensively addressed for their successful real-world application. Analytical robustness remains a major concern, as poor specificity and non-specific interactions in complex biological samples can lead to false positives or negatives. MNPs such as AgNPs, are also prone to oxidation, aggregation, and photodegradation, limiting shelf life and performance consistency, especially on porous paper substrates.

Colorimetric outputs, while popular for their simplicity and equipment-free operation, often lack sensitivity and quantification, hindered by uneven reagent distribution, subjective interpretation, and background noise. Additionally, variations in nanoparticle synthesis and unstable signal generation reduce reliability. Fluid control is another notable challenge. The capillary flow is sensitive to environmental fluctuations and substrate inconsistencies, complicating multistep assays. Fabrication challenges remain significant, as current methods like wax printing and inkjet deposition often lack the precision and scalability needed for mass production without compromising MNP functionality.

For commercialization, technological fragmentation persists, as diverse MNP based sensing principles lack standardization. This absence of unified protocols hinders the





development of modular device designs, interoperability, and the potential for reuse, making it difficult to scale up or adapt devices across different applications. Most  $\mu$ PADs lack programmable microfluidic elements for controlled reagent delivery, while critical metrics like long-term stability, user variability, and clinical validation are often underexplored. As a result, reaching clinical or commercial maturity remains a significant challenge for MNP integrated  $\mu$ PADs, due to fragmented design processes and insufficient user-focused optimization. Additionally, despite their promising capabilities, research on microfluidic paper-based SERS platforms remains surprisingly limited.

To accelerate the commercialization of MNP integrated  $\mu$ PADs, a systematic approach is essential, addressing these critical challenges through targeted technological, and user-centered strategies. To overcome poor specificity and false positives, advanced surface functionalization techniques should be employed to immobilize highly selective biorecognition elements (e.g., monoclonal antibodies, aptamers, or molecularly imprinted polymers) directly onto MNP surfaces. Additionally, multi-modal sensing approaches, which combine optical with electrochemical or electrochemiluminescent outputs, can cross-validate signals and significantly improve reliability within complex biological matrices. To enhance stability and extend shelf life, the encapsulation of MNPs using polymeric coatings, or embedding within hydrogel matrices can effectively protect them from oxidation, aggregation, and photodegradation.

For quantitative and consistent outputs, especially in colorimetry, the incorporation of digital image analysis via smartphone applications or portable readers can standardize results and reduce human error. Furthermore, adopting batch-controlled nanoparticle synthesis protocols with narrow size and shape distributions can significantly improve consistency. To address fluid control challenges, advanced microfluidic channel engineering such as the use of wax barriers, 3D origami designs, or programmable hydrogels can precisely regulate reagent timing, mixing, and flow. Incorporating valves, spacers, and reservoirs into layered  $\mu$ PADs or utilizing hydrophobic patterning can minimize variability due to humidity or temperature fluctuations and effectively support multistep reactions.

Bridging the translation gap and achieving successful commercialization requires cross-sector collaboration among academic researchers, device manufacturers, and healthcare providers. The path forward involves transforming laboratory-scale innovations into robust, standardized, and user-friendly diagnostic platforms through a multidisciplinary effort that combines materials science, microfluidics, nanotechnology, clinical validation, and systems engineering. The authors believe that by effectively addressing these outlined technical and translational bottlenecks, MNP integrated  $\mu$ PADs hold the potential to deliver scalable, affordable, and reliable tools for global healthcare and environmental monitoring. The rapid progress in nanomaterials and nanotechnology is expected to lead to devices with higher sensitivity, improved signal transduction, and the ability to detect multiple analytes

simultaneously. Future advancements will likely focus on efficient MNP immobilization within paper matrices and the targeted trapping and pre-concentration of target analytes. In the coming years, these low-cost and efficient diagnostic platforms are anticipated to become essential tools across various healthcare settings, including clinics, laboratories, nursing homes, hospitals, and even bedside care. Ultimately, they are poised to make a profound global health impact by enabling accessible disease detection in developing regions and resource-constrained environments.

## Conflicts of interest

There are no conflicts of interest to declare.

## Data availability

No primary research results, software or code have been included and no new data were generated or analysed as part of this review.

## References

- 1 B. Srinivasan and S. Tung, *SLAS Technol.*, 2015, **20**, 365–389.
- 2 I. A. Quintela, T. Vasse, C. S. Lin and V. C. H. Wu, *Front. Microbiol.*, 2022, **13**, 1054782.
- 3 C. Parolo and A. Merkoçi, *Chem. Soc. Rev.*, 2013, **42**, 450–457.
- 4 F. Ghasemi, N. Fahimi-Kashani, A. Bigdeli, A. H. Alshatteri, S. Abbasi-Moayed, S. H. Al-Jaf, M. Y. Merry, K. M. Omer and M. R. Hormozi-Nezhad, *Anal. Chim. Acta*, 2023, **1238**, 340640.
- 5 Z. Wang, Y.-H. Lee, S.-W. Kim, J.-Y. Seo, S.-Y. Lee and L. Nyholm, *Adv. Mater.*, 2021, **33**, 2000892.
- 6 A. Kumar and P. Maiti, *Mater. Adv.*, 2024, **5**, 3563–3586.
- 7 A. H. Free, E. C. Adams, M. L. Kercher, H. M. Free and M. H. Cook, *Clin. Chem.*, 1957, **3**, 163–168.
- 8 E. M. Fenton, M. R. Mascarenas, G. P. López and S. S. Sibbett, *ACS Appl. Mater. Interfaces*, 2009, **1**, 124–129.
- 9 E. Carrilho, S. T. Phillips, S. J. Vella, A. W. Martinez and G. M. Whitesides, *Anal. Chem.*, 2009, **81**, 5990–5998.
- 10 A. K. Yetisen, M. S. Akram and C. R. Lowe, *Lab Chip*, 2013, **13**, 2210–2251.
- 11 A. R. Rezk, A. Qi, J. R. Friend, W. H. Li and L. Y. Yeo, *Lab Chip*, 2012, **12**, 773–779.
- 12 P. K. Jain and M. A. El-Sayed, *Chem. Phys. Lett.*, 2010, **487**, 153–164.
- 13 A. Meola, J. Rao, N. Chaudhary, M. Sharma and S. D. Chang, *Front. Neurol.*, 2018, **9**, 328.
- 14 Y. Cheng, L. Yin, S. Lin, M. Wiesner, E. Bernhardt and J. Liu, *J. Phys. Chem. C*, 2011, **115**, 4425–4432.
- 15 M. A. Garcia, *J. Phys. D: Appl. Phys.*, 2011, **44**, 283001.
- 16 N. Lopez-Ruiz, V. F. Curto, M. M. Erenas, F. Benito-Lopez, D. Diamond, A. J. Palma and L. F. Capitán-Vallvey, *Anal. Chem.*, 2014, **86**, 9554–9562.



- 17 S. Rasheed, N. Ahmad, A. Nafady, M. Anwar Ul Haq, T. Kanwal, R. Mujeeb ur, D. Hussain, S. Uddin and R. Ali Soomro, *Measurement*, 2025, **239**, 115519.
- 18 E. Noviana, T. Ozer, C. S. Carrell, J. S. Link, C. McMahon, I. Jang and C. S. Henry, *Chem. Rev.*, 2021, **121**, 11835–11885.
- 19 W. Li, X. Ma, Y.-C. Yong, G. Liu and Z. Yang, *Anal. Chim. Acta*, 2023, **1278**, 341614.
- 20 D. M. Cate, J. A. Adkins, J. Mettakoonpitak and C. S. Henry, *Anal. Chem.*, 2015, **87**, 19–41.
- 21 S. Marquez and E. Morales-Narváez, *Front. bioeng. biotechnol.*, 2019, **7**, 69.
- 22 M. J. Oliveira, A. Dalot, E. Fortunato, R. Martins, H. J. Byrne, R. Franco and H. Águas, *Discover Mater.*, 2022, **2**, 12.
- 23 S. Chupradit, M. Kavitha, W. Suksatan, M. J. Ansari, Z. I. Al Mashhadani, M. M. Kadhimi, Y. F. Mustafa, S. S. Shafik and E. Kianfar, *Adv. Mater. Sci. Eng.*, 2022, **2022**, 1971891.
- 24 A. Corma and H. Garcia, *Chem. Soc. Rev.*, 2008, **37**, 2096–2126.
- 25 V. V. Mody, R. Siwale, A. Singh and H. R. Mody, *J. Pharm. BioAllied Sci.*, 2010, **2**, 282–289.
- 26 M.-C. Daniel and D. Astruc, *Chem. Rev.*, 2004, **104**, 293–346.
- 27 K. L. Kelly, E. Coronado, L. L. Zhao and G. C. Schatz, *J. Phys. Chem. B*, 2003, **107**, 668–677.
- 28 M. Pelton, J. Aizpurua and G. Bryant, *Laser Photonics Rev.*, 2008, **2**, 136–159.
- 29 L. Lin, X. Bi, Y. Gu, F. Wang and J. Ye, *J. Appl. Phys.*, 2021, **129**, 191101.
- 30 E. Ozbay, *Science*, 2006, **311**, 189–193.
- 31 D. K. Gramotnev and S. I. Bozhevolnyi, *Nat. Photonics*, 2010, **4**, 83–91.
- 32 J. Zhou, Y. Wang, L. Zhang and X. Li, *Chin. Chem. Lett.*, 2018, **29**, 54–60.
- 33 J. M. Luther, P. K. Jain, T. Ewers and A. P. Alivisatos, *Nat. Mater.*, 2011, **10**, 361–366.
- 34 Y. Li, P. Ferreyra, A. K. Swan and R. Paiella, *ACS Photonics*, 2019, **6**, 2562–2569.
- 35 T. R. Jensen, M. D. Malinsky, C. L. Haynes and R. P. Van Duyne, *J. Phys. Chem. B*, 2000, **104**, 10549–10556.
- 36 N. Gisbert Quilis, M. van Dongen, P. Venugopalan, D. Kotlarek, C. Petri, A. Moreno Cencerrado, S. Stanesco, J. L. Toca Herrera, U. Jonas and M. Möller, *Adv. Opt. Mater.*, 2019, **7**, 1900342.
- 37 W. Hergert and T. Wriedt, *The Mie Theory: Basics and Applications*, Springer Berlin Heidelberg, 2012.
- 38 G. Mie, *Ann. Phys.*, 1908, **330**, 377–445.
- 39 W. H. Yang, G. C. Schatz and R. P. Van Duyne, *J. Chem. Phys.*, 1995, **103**, 869–875.
- 40 T. R. Jensen, M. L. Duval, K. L. Kelly, A. A. Lazarides, G. C. Schatz and R. P. Van Duyne, *J. Phys. Chem. B*, 1999, **103**, 9846–9853.
- 41 P. Venugopalan and S. kumar, *Opt. Mater. Express*, 2022, **12**, 2127–2134.
- 42 K. M. Mayer and J. H. Hafner, *Chem. Rev.*, 2011, **111**, 3828–3857.
- 43 J. Jatschka, A. Dathe, A. Csáki, W. Fritzsche and O. Stranik, *Sens. Bio-Sens. Res.*, 2016, **7**, 62–70.
- 44 M. Katagiri, J. L. Cuya Huaman, T. Matsumoto, K. Suzuki, H. Miyamura and J. Balachandran, *ACS Appl. Nano Mater.*, 2020, **3**, 418–427.
- 45 J. He, L. Ai, X. Liu, H. Huang, Y. Li, M. Zhang, Q. Zhao, X. Wang, W. Chen and H. Gu, *J. Mater. Chem. B*, 2018, **6**, 1035–1043.
- 46 N. S. S. Mousavi, K. B. Ramadi, Y.-A. Song and S. Kumar, *Commun. Mater.*, 2023, **4**, 101.
- 47 P. Venugopalan, Q. Zhang, X. Li, L. Kuipers and M. Gu, *Opt. Lett.*, 2014, **39**, 5744–5747.
- 48 P. Venugopalan, Q. Zhang, X. Li and M. Gu, *Opt. Express*, 2013, **21**, 15247–15252.
- 49 R. Zhang, Y. Zhang, Z. C. Dong, S. Jiang, C. Zhang, L. G. Chen, L. Zhang, Y. Liao, J. Aizpurua, Y. Luo, J. L. Yang and J. G. Hou, *Nature*, 2013, **498**, 82–86.
- 50 L. Piatkowski, N. Accanto and N. F. van Hulst, *ACS Photonics*, 2016, **3**, 1401–1414.
- 51 R.-M. Ma, S. Ota, Y. Li, S. Yang and X. Zhang, *Nat. Nanotechnol.*, 2014, **9**, 600–604.
- 52 J. Zeng and Y. Xuan, *Nano Energy*, 2018, **51**, 754–763.
- 53 M. Chen, F. Y. H. Kutsanedzie, W. Cheng, H. Li and Q. Chen, *Microchem. J.*, 2019, **144**, 296–302.
- 54 D. T. Thompson, *Nano Today*, 2007, **2**, 40–43.
- 55 S. A. Jasim, M. M. Kadhimi, V. Kn, I. Raya, S. J. Shoja, W. Suksatan, M. H. Ali and e. kianfar, *Braz. J. Phys.*, 2022, **52**, 31.
- 56 Z. Ma, X. Zhang, X. Guo, Q. Yang, Y. Ma and L. Tong, *Appl. Phys. Lett.*, 2010, **96**, 051119.
- 57 J. L. Delaney, C. F. Hogan, J. Tian and W. Shen, *Anal. Chem.*, 2011, **83**, 1300–1306.
- 58 J. Adkins, K. Boehle and C. Henry, *Electrophoresis*, 2015, **36**, 1811–1824.
- 59 T. V. António, A. Andreia, G. Diana, S. Lídia, C. M. Ana, J. M. Manuel, P. Luís, F. Elvira and M. Rodrigo, in *Nanostructured Solar Cells*, ed. D. Narottam, IntechOpen, Rijeka, 2017, DOI: [10.5772/66695](https://doi.org/10.5772/66695).
- 60 D. Tobjörk and R. Österbacka, *Adv. Mater.*, 2011, **23**, 1935–1961.
- 61 K. Yuwawech, J. Wootthikanokkhan and S. Tanpichai, *Polym. Test.*, 2015, **48**, 12–22.
- 62 X. Du, Z. Zhang, W. Liu and Y. Deng, *Nano Energy*, 2017, **35**, 299–320.
- 63 E. Małachowska, M. Dubowik, P. Boruszewski, J. Łojewska and P. Przybysz, *Sci. Rep.*, 2020, **10**, 19998.
- 64 E. Małachowska, M. Dubowik, P. Boruszewski and P. Przybysz, *Heritage Sci.*, 2021, **9**, 132.
- 65 L. Hu, G. Zheng, J. Yao, N. Liu, B. Weil, M. Eskilsson, E. Karabulut, Z. Ruan, S. Fan, J. T. Bloking, M. D. McGehee, L. Wågberg and Y. Cui, *Energy Environ. Sci.*, 2013, **6**, 513–518.
- 66 H. P. S. Abdul Khalil, A. H. Bhat and A. F. Ireana Yusra, *Carbohydr. Polym.*, 2012, **87**, 963–979.
- 67 R. J. Moon, A. Martini, J. Nairn, J. Simonsen and J. Youngblood, *Chem. Soc. Rev.*, 2011, **40**, 3941–3994.
- 68 K.-Y. Lee, G. Buldum, A. Mantalaris and A. Bismarck, *Macromol. Biosci.*, 2014, **14**, 10–32.



- 69 Z. Fang, H. Zhu, C. Preston and L. Hu, *Transl. Mater. Res.*, 2014, **1**, 015004.
- 70 N. Sharma, T. Barstis and B. Giri, *Eur. J. Pharm. Sci.*, 2018, **111**, 46–56.
- 71 M. Wu, P. Li, Q. Zhu, M. Wu, H. Li and F. Lu, *Spectrochim. Acta, Part A*, 2018, **196**, 110–116.
- 72 R. Alder, J. Hong, E. Chow, J. Fang, F. Isa, B. Ashford, C. Comte, A. Bendavid, L. Xiao, K. K. Ostrikov, S. Fu and A. B. Murphy, *Sensors*, 2021, **21**, 810.
- 73 R. Pelton, *TrAC, Trends Anal. Chem.*, 2009, **28**, 925–942.
- 74 A. W. Martinez, S. T. Phillips, G. M. Whitesides and E. Carrilho, *Anal. Chem.*, 2010, **82**, 3–10.
- 75 W. W. Yu and I. M. White, *Anal. Chem.*, 2010, **82**, 9626–9630.
- 76 Z. Dai, X. Xiao, W. Wu, L. Liao, F. Mei, X. Yu, S. Guo, J. Ying, F. Ren and C. Jiang, *Appl. Phys. Lett.*, 2014, **105**, 211902.
- 77 W. W. Yu and I. M. White, *Analyst*, 2013, **138**, 1020–1025.
- 78 G. Yang, X. Fang, Q. Jia, H. Gu, Y. Li, C. Han and L.-L. Qu, *Microchim. Acta*, 2020, **187**, 310.
- 79 M. J. Oliveira, P. Quaresma, M. Peixoto de Almeida, A. Araújo, E. Pereira, E. Fortunato, R. Martins, R. Franco and H. Águas, *Sci. Rep.*, 2017, **7**, 2480.
- 80 D.-J. Lee and D. Y. Kim, *Sensors*, 2019, **19**, 5471.
- 81 Y. H. Ngo, D. Li, G. P. Simon and G. Garnier, *Langmuir*, 2012, **28**, 8782–8790.
- 82 M.-L. Cheng, B.-C. Tsai and J. Yang, *Anal. Chim. Acta*, 2011, **708**, 89–96.
- 83 G. Zheng, L. Polavarapu, L. M. Liz-Marzán, I. Pastoriza-Santos and J. Pérez-Juste, *Chem. Commun.*, 2015, **51**, 4572–4575.
- 84 L. F. Sallum, F. L. F. Soares, J. A. Ardila and R. L. Carneiro, *Spectrochim. Acta, Part A*, 2014, **133**, 107–111.
- 85 K. Castro, E. Princi, N. Proietti, M. Manso, D. Capitani, S. Vicini, J. M. Madariaga and M. L. De Carvalho, *Nucl. Instrum. Methods Phys. Res., Sect. B*, 2011, **269**, 1401–1410.
- 86 Y. Li, K. Zhang, J. Zhao, J. Ji, C. Ji and B. Liu, *Talanta*, 2016, **147**, 493–500.
- 87 J. Hong, S. Yick, E. Chow, A. Murdock, J. Fang, D. H. Seo, A. Wolff, Z. Han, T. van der Laan, A. Bendavid, K. Ostrikov and A. B. Murphy, *J. Mater. Chem. C*, 2019, **7**, 6369–6374.
- 88 R. Zhang, B.-B. Xu, X.-Q. Liu, Y.-L. Zhang, Y. Xu, Q.-D. Chen and H.-B. Sun, *Chem. Commun.*, 2012, **48**, 5913–5915.
- 89 D. Gaspar, A. C. Pimentel, T. Mateus, J. P. Leitão, J. Soares, B. P. Falcão, A. Araújo, A. Vicente, S. A. Filonovich, H. Águas, R. Martins and I. Ferreira, *Sci. Rep.*, 2013, **3**, 1469.
- 90 T. Vo-Dinh, M. Y. K. Hiromoto, G. M. Begun and R. L. Moody, *Anal. Chem.*, 1984, **56**, 1667–1670.
- 91 A. Araújo, C. Caro, M. J. Mendes, D. Nunes, E. Fortunato, R. Franco, H. Águas and R. Martins, *Nanotechnology*, 2014, **25**, 415202.
- 92 A. Araújo, A. Pimentel, M. J. Oliveira, M. J. Mendes, R. Franco, E. Fortunato, H. Águas and R. Martins, *Flexible Printed Electron.*, 2017, **2**, 014001.
- 93 S.-C. Tseng, C.-C. Yu, D. Wan, H.-L. Chen, L. A. Wang, M.-C. Wu, W.-F. Su, H.-C. Han and L.-C. Chen, *Anal. Chem.*, 2012, **84**, 5140–5145.
- 94 H. Yingying, X. Jiangtao, Z. Sihang, L. Zhichao, M. Dagang and J. Shouxiang, *Microchem. J.*, 2024, **196**, 109700.
- 95 Y. Zhu, L. Zhang and L. Yang, *Mater. Res. Bull.*, 2015, **63**, 199–204.
- 96 S. Smith, K. Govindasamy, U. Govender, H. Chen, L. Fourie, S. Ngwenya, S. Kumar, P. Mjwana, H. Cele, M. Mbanjwa, S. Potgieter, T. Joubert and K. Land, *S. Afr. J. Sci.*, 2015, **111**, 10.
- 97 M. M. Hamed, A. Ainla, F. Güder, D. C. Christodouleas, M. T. Fernández-Abedul and G. M. Whitesides, *Adv. Mater.*, 2016, **28**, 5054–5063.
- 98 D. D. Liana, B. Raguse, J. J. Gooding and E. Chow, *Sensors*, 2012, **12**, 11505–11526.
- 99 A. H. Gordon, A. J. Martin and R. L. Synge, *Biochem. J.*, 1943, **37**, 79–86.
- 100 A. W. Martinez, S. T. Phillips, M. J. Butte and G. M. Whitesides, *Angew. Chem., Int. Ed.*, 2007, **46**, 1318–1320.
- 101 A. A. Benson, *J. Am. Chem. Soc.*, 1958, **80**, 5010.
- 102 A. K. Ellerbee, S. T. Phillips, A. C. Siegel, K. A. Mirica, A. W. Martinez, P. Striehl, N. Jain, M. Prentiss and G. M. Whitesides, *Anal. Chem.*, 2009, **81**, 8447–8452.
- 103 E. Evans, E. F. M. Gabriel, W. K. T. Coltro and C. D. Garcia, *Analyst*, 2014, **139**, 2127–2132.
- 104 D. Mark, S. Haeberle, G. Roth, F. Von Stetten and R. Zengerle, *Chem. Soc. Rev.*, 2010, **39**, 1153–1182.
- 105 T. Akyazi, L. Basabe-Desmonts and F. Benito-Lopez, *Anal. Chim. Acta*, 2018, **1001**, 1–17.
- 106 J. Hu, S. Wang, L. Wang, F. Li, B. Pingguan-Murphy, T. J. Lu and F. Xu, *Biosens. Bioelectron.*, 2014, **54**, 585–597.
- 107 M. E. I. Badawy and A. F. El-Aswad, *Int. J. Anal. Chem.*, 2014, **2014**, 536823.
- 108 L. Rivas, M. Medina-Sánchez, A. de la Escosura-Muñiz and A. Merkoçi, *Lab Chip*, 2014, **14**, 4406–4414.
- 109 V. Shirshahi and Z. B. Afrapoli, in *Comprehensive Analytical Chemistry*, ed. C. Mustansar Hussain, Elsevier, 2024, vol. 105, pp. 301–330.
- 110 S. Wang, L. Ge, X. Song, J. Yu, S. Ge, J. Huang and F. Zeng, *Biosens. Bioelectron.*, 2012, **31**, 212–218.
- 111 C.-M. Cheng, A. W. Martinez, J. Gong, C. R. Mace, S. T. Phillips, E. Carrilho, K. A. Mirica and G. M. Whitesides, *Angew. Chem., Int. Ed.*, 2010, **49**, 4771–4774.
- 112 P. Kwong and M. Gupta, *Anal. Chem.*, 2012, **84**, 10129–10135.
- 113 G. Demirel and E. Babur, *Analyst*, 2014, **139**, 2326–2331.
- 114 T. Lam, J. P. Devadhasan, R. Howse and J. Kim, *Sci. Rep.*, 2017, **7**, 1188.
- 115 W. Dungchai, O. Chailapakul and C. S. Henry, *Analyst*, 2011, **136**, 77–82.
- 116 C. Renault, J. Koehne, A. J. Ricco and R. M. Crooks, *Langmuir*, 2014, **30**, 7030–7036.
- 117 Y. Matsuda, S. Shibayama, K. Uete, H. Yamaguchi and T. Niimi, *Anal. Chem.*, 2015, **87**, 5762–5765.
- 118 W. Y. Lim, C.-H. Goh, K. Z. Yap and N. Ramakrishnan, *Biosensors*, 2023, **13**, 209.





- 119 K. Maejima, S. Tomikawa, K. Suzuki and D. Citterio, *RSC Adv.*, 2013, **3**, 9258–9263.
- 120 K. Abe, K. Suzuki and D. Citterio, *Anal. Chem.*, 2008, **80**, 6928–6934.
- 121 J. S. Ng and M. Hashimoto, *RSC Adv.*, 2020, **10**, 29797–29807.
- 122 P. Spicar-Mihalic, B. Toley, J. Houghtaling, T. Liang, P. Yager and E. Fu, *J. Micromech. Microeng.*, 2013, **23**, 067003.
- 123 N. Kumawat, S. S. Soman, S. Vijayavenkataraman and S. Kumar, *Lab Chip*, 2022, **22**, 3377–3389.
- 124 W. Zhao, M. M. Ali, S. D. Aguirre, M. A. Brook and Y. Li, *Anal. Chem.*, 2008, **80**, 8431–8437.
- 125 S. Lou, J.-y. Ye, K.-q. Li and A. Wu, *Analyst*, 2012, **137**, 1174–1181.
- 126 S. Puertas, M. Moros, R. Fernández-Pacheco, M. R. Ibarra, V. Grazú and J. M. de la Fuente, *J. Phys. D: Appl. Phys.*, 2010, **43**, 474012.
- 127 X. Zhu, L. Chen, P. Shen, J. Jia, D. Zhang and L. Yang, *J. Agric. Food Chem.*, 2011, **59**, 2184–2189.
- 128 S. Shukla, H. Leem and M. Kim, *Anal. Bioanal. Chem.*, 2011, **401**, 2581–2590.
- 129 M. Blažková, B. Javůrková, L. Fukal and P. Rauch, *Biosens. Bioelectron.*, 2011, **26**, 2828–2834.
- 130 J. Li and J. Macdonald, *Lab Chip*, 2016, **16**, 242–245.
- 131 M. A. Morales and J. M. Halpern, *Bioconjugate Chem.*, 2018, **29**, 3231–3239.
- 132 L. C. Brazaca, J. R. Moreto, A. Martín, F. Tehrani, J. Wang and V. Zucolotto, *ACS Nano*, 2019, **13**, 13325–13332.
- 133 V. Hamedpour, G. J. Postma, E. van den Heuvel, J. J. Jansen, K. Suzuki and D. Citterio, *Anal. Bioanal. Chem.*, 2018, **410**, 2305–2313.
- 134 K. Khachornsakkul, R. Del-Rio-Ruiz, H. Creasey, G. Widmer and S. R. Sonkusale, *ACS Sens.*, 2023, **8**, 4364–4373.
- 135 P. Nath, R. K. Arun and N. Chanda, *RSC Adv.*, 2014, **4**, 59558–59561.
- 136 T. Ming, J. Luo, J. Liu, S. Sun, Y. Xing, H. Wang, G. Xiao, Y. Deng, Y. Cheng, Z. Yang, H. Jin and X. Cai, *Biosens. Bioelectron.*, 2020, **170**, 112649.
- 137 L. Zhang, Y. Yang, J. Tan and Q. Yuan, *Mater. Chem. Front.*, 2020, **4**, 1315–1327.
- 138 S. B. Somvanshi, A. M. Ulloa, M. Zhao, Q. Liang, A. K. Barui, A. Lucas, K. M. Jadhav, J. P. Allebach and L. A. Stanciu, *Biosens. Bioelectron.*, 2022, **207**, 114214.
- 139 G.-H. Chen, W.-Y. Chen, Y.-C. Yen, C.-W. Wang, H.-T. Chang and C.-F. Chen, *Anal. Chem.*, 2014, **86**, 6843–6849.
- 140 S. Shariati and G. Khayatian, *New J. Chem.*, 2020, **44**, 18662–18667.
- 141 A. Scroccarello, F. Della Pelle, D. Rojas, G. Ferraro, E. Fratini, S. Gaggiotti, A. Cichelli and D. Compagnone, *Anal. Chim. Acta*, 2021, **1183**, 338971.
- 142 M.-R. Xie, Y. Cai, Y.-Q. Liu and Z.-Y. Wu, *Talanta*, 2020, **212**, 120749.
- 143 L. Wang and B. McCord, *Anal. Biochem.*, 2020, **595**, 113619.
- 144 B. Heli, E. Morales-Narváez, H. Golmohammadi, A. Ajji and A. Merkoçi, *Nanoscale*, 2016, **8**, 7984–7991.
- 145 J. Yu, L. Ge, J. Huang, S. Wang and S. Ge, *Lab Chip*, 2011, **11**, 1286–1291.
- 146 N. Ruecha, N. Rodthongkum, D. M. Cate, J. Volckens, O. Chailapakul and C. S. Henry, *Anal. Chim. Acta*, 2015, **874**, 40–48.
- 147 S. S. Soman, S. A. Samad, P. Venugopalan, N. Kumawat and S. Kumar, *BiOMICROFLUIDICS*, 2024, **18**, 031501.
- 148 K. Yang, H. Peretz-Soroka, Y. Liu and F. Lin, *Lab Chip*, 2016, **16**, 943–958.
- 149 L. Shen, J. A. Hagen and I. Papautsky, *Lab Chip*, 2012, **12**, 4240–4243.
- 150 E. Celikbas, E. Guler Celik and S. Timur, *Anal. Chem.*, 2018, **90**, 12325–12333.
- 151 A. W. Martinez, S. T. Phillips, E. Carrilho, S. W. Thomas, III, H. Sindi and G. M. Whitesides, *Anal. Chem.*, 2008, **80**, 3699–3707.
- 152 D.-S. Lee, B. G. Jeon, C. Ihm, J.-K. Park and M. Y. Jung, *Lab Chip*, 2011, **11**, 120–126.
- 153 Y.-S. Li and J. S. Church, *J. Food Drug Anal.*, 2014, **22**, 29–48.
- 154 R. S. Krishnan and R. K. Shankar, *J. Raman Spectrosc.*, 1981, **10**, 1–8.
- 155 C. V. Raman and K. S. Krishnan, *Nature*, 1928, **121**, 501–502.
- 156 C. L. Haynes, A. D. McFarland and R. P. Van Duyne, *Anal. Chem.*, 2005, **77**, 338A–346A.
- 157 A. J. McQuillan, *Notes Rec. R. Soc. Lond.*, 2009, **63**, 105–109.
- 158 M. Fleischmann, P. J. Hendra and A. J. McQuillan, *Chem. Phys. Lett.*, 1974, **26**, 163–166.
- 159 D. L. Jeanmaire and R. P. Van Duyne, *J. Electroanal. Chem. Interfacial Electrochem.*, 1977, **84**, 1–20.
- 160 M. G. Albrecht and J. A. Creighton, *J. Am. Chem. Soc.*, 1977, **99**, 5215–5217.
- 161 S. Nie and S. R. Emory, *Science*, 1997, **275**, 1102–1106.
- 162 S. Schlücker, *Angew Chem. Int. Ed. Engl.*, 2014, **53**, 4756–4795.
- 163 F. J. García-Vidal and J. B. Pendry, *Phys. Rev. Lett.*, 1996, **77**, 1163–1166.
- 164 J. Kim, Y. Jang, N. J. Kim, H. Kim, G. C. Yi, Y. Shin, M. H. Kim and S. Yoon, *Front. Chem.*, 2019, **7**, 582.
- 165 M. F. Cardinal, E. Vander Ende, R. A. Hackler, M. O. McAnally, P. C. Stair, G. C. Schatz and R. P. Van Duyne, *Chem. Soc. Rev.*, 2017, **46**, 3886–3903.
- 166 S. M. Stranahan and K. A. Willets, *Nano Lett.*, 2010, **10**, 3777–3784.
- 167 J. Theiss, P. Pavaskar, P. M. Echternach, R. E. Muller and S. B. Cronin, *Nano Lett.*, 2010, **10**, 2749–2754.
- 168 A. X. Wang and X. Kong, *Materials*, 2015, **8**, 3024–3052.
- 169 W.-H. Park and Z. H. Kim, *Nano Lett.*, 2010, **10**, 4040–4048.
- 170 S. Lecomte, P. Matejka and M. H. Baron, *Langmuir*, 1998, **14**, 4373–4377.
- 171 A. Otto, I. Mrozek, H. Grabhorn and W. Akemann, *J. Phys.: Condens. Matter*, 1992, **4**, 1143.
- 172 R. Pilot, R. Signorini, C. Durante, L. Orian, M. Bhamidipati and L. Fabris, *Biosensors*, 2019, **9**.
- 173 C. Li, Y. Huang, X. Li, Y. Zhang, Q. Chen, Z. Ye, Z. Alqarni, S. E. J. Bell and Y. Xu, *J. Mater. Chem. C*, 2021, **9**, 11517–11552.



- 174 A. M. Robinson, L. Zhao, M. Y. Shah Alam, P. Bhandari, S. G. Harroun, D. Dendukuri, J. Blackburn and C. L. Brosseau, *Analyst*, 2015, **140**, 779–785.
- 175 C. Liu, D. Xu, X. Dong and Q. Huang, *Trends Food Sci. Technol.*, 2022, **128**, 90–101.
- 176 M. Fan, G. F. S. Andrade and A. G. Brolo, *Anal. Chim. Acta*, 2020, **1097**, 1–29.
- 177 T. Vo-Dinh, *TrAC, Trends Anal. Chem.*, 1998, **17**, 557–582.
- 178 V. A. Tran, T. T. V. Tran, V. T. Le, V. D. Doan, G. N. L. Vo, V. H. Tran, H. Jeong and T. T. T. Vo, *Appl. Mater. Today*, 2024, **38**, 102217.
- 179 K. A. Stoerzinger, J. Y. Lin and T. W. Odom, *Chem. Sci.*, 2011, **2**, 1435–1439.
- 180 H. Liu, L. Yang and J. Liu, *TrAC, Trends Anal. Chem.*, 2016, **80**, 364–372.
- 181 S. Liu and Z. Tang, *J. Mater. Chem.*, 2010, **20**, 24–35.
- 182 N. G. Quilis, M. Lequeux, P. Venugopalan, I. Khan, W. Knoll, S. Boujday, M. L. de La Chapelle and J. Dostalek, *Nanoscale*, 2018, **10**, 10268–10276.
- 183 Z. Zhu, H. Meng, W. Liu, X. Liu, J. Gong, X. Qiu, L. Jiang, D. Wang and Z. Tang, *Angew Chem. Int. Ed. Engl.*, 2011, **50**, 1593–1596.
- 184 Á. I. López-Lorente, *Anal. Chim. Acta*, 2021, **1168**, 338474.
- 185 V. Kaushik, H. L. Kagdada, D. K. Singh and S. Pathak, *Appl. Surf. Sci.*, 2022, **574**, 151724.
- 186 M. Rycenga, C. M. Cobley, J. Zeng, W. Li, C. H. Moran, Q. Zhang, D. Qin and Y. Xia, *Chem. Rev.*, 2011, **111**, 3669–3712.
- 187 W. Wang, P. Ma and D. Song, *Luminescence*, 2022, **37**, 1822–1835.
- 188 A. T. Vicente, A. Araújo, M. J. Mendes, D. Nunes, M. J. Oliveira, O. Sanchez-Sobrado, M. P. Ferreira, H. Águas, E. Fortunato and R. Martins, *J. Mater. Chem. C*, 2018, **6**, 3143–3181.
- 189 C. H. Lee, L. Tian and S. Singamaneni, *ACS Appl. Mater. Interfaces*, 2010, **2**, 3429–3435.
- 190 J. Xie, L. Li, I. M. Khan, Z. Wang and X. Ma, *Spectrochim. Acta, Part A*, 2020, **231**, 118104.
- 191 K. Ren, J. Zhou and H. Wu, *Acc. Chem. Res.*, 2013, **46**, 2396–2406.
- 192 L. Polavarapu, A. L. Porta, S. M. Novikov, M. Coronado-Puchau and L. M. Liz-Marzán, *Small*, 2014, **10**, 3065–3071.
- 193 A. Martín, J. J. Wang and D. Iacopino, *RSC Adv.*, 2014, **4**, 20038–20043.
- 194 B. Li, W. Zhang, L. Chen and B. Lin, *Electrophoresis*, 2013, **34**, 2162–2168.
- 195 A. Saha and N. R. Jana, *ACS Appl. Mater. Interfaces*, 2015, **7**, 996–1003.
- 196 H. Torul, H. Çiftçi, D. Çetin, Z. Suludere, I. H. Boyacı and U. Tamer, *Anal. Bioanal. Chem.*, 2015, **407**, 8243–8251.
- 197 M. Chen, H. Yang, L. Rong and X. Chen, *Analyst*, 2016, **141**, 5511–5519.
- 198 J.-C. Lee, W. Kim and S. Choi, *Int. J. Precis. Eng. Manuf. - Green Technol.*, 2017, **4**, 221–226.
- 199 W. Kim, Y.-H. Kim, H.-K. Park and S. Choi, *ACS Appl. Mater. Interfaces*, 2015, **7**, 27910–27917.
- 200 M. Sharipov, T. J. Ju, S. Azizov, A. Turaev and Y. I. Lee, *J. Hazard. Mater.*, 2024, **461**, 132561.
- 201 L.-A. Wu, K.-T. Hsieh, C.-S. Lin, Y.-L. Wang and Y.-F. Chen, *Microfluid. Nanofluid.*, 2024, **28**, 57.
- 202 J. Zhuang, Z. Zhao, K. Lian, L. Yin, J. Wang, S. Man, G. Liu and L. Ma, *Biosens. Bioelectron.*, 2022, **207**, 114167.
- 203 T. K. Naqvi, A. Bajpai, S. Dwivedi, M. Bhaiyya, S. Goel and P. K. Dwivedi, *Sens. Actuators, A*, 2023, **356**, 114341.
- 204 J. Zhu, Q. Chen, F. Y. H. Kutsanedzie, M. Yang, Q. Ouyang and H. Jiang, *Anal. Methods*, 2017, **9**, 6186–6193.
- 205 F. Zeng, W. Duan, B. Zhu, T. Mu, L. Zhu, J. Guo and X. Ma, *Anal. Chem.*, 2019, **91**, 1064–1070.
- 206 S. Mabbott, S. C. Fernandes, M. Schechinger, G. L. Cote, K. Faulds, C. R. Mace and D. Graham, *Analyst*, 2020, **145**, 983–991.
- 207 A. Teixeira, J. F. Hernández-Rodríguez, L. Wu, K. Oliveira, K. Kant, P. Piairo, L. Diéguez and S. Abalde-Cela, *Appl. Sci.*, 2019, **9**, 1387.
- 208 W. Y. Lim, C.-H. Goh, T. M. Thevarajah, B. T. Goh and S. M. Khor, *Biosens. Bioelectron.*, 2020, **147**, 111792.
- 209 U. Mogera, H. Guo, M. Namkoong, M. S. Rahman, T. Nguyen and L. Tian, *Sci. Adv.*, 2022, **8**, eabn1736.
- 210 M. Liu, H. Zhang, J. Shu, X. Liu, F. Li and H. Cui, *Anal. Chem.*, 2014, **86**, 2857–2861.
- 211 W. Liu, J. Luo, Y. Guo, J. Kou, B. Li and Z. Zhang, *Talanta*, 2014, **120**, 336–341.
- 212 L. Zhao, J. Xu, L. Xiong, S. Wang, C. Yu, J. Lv and J.-M. Lin, *TrAC, Trends Anal. Chem.*, 2023, **166**, 117213.
- 213 Y. Lu, J. Xu, D. J. Riley and F. Xie, *J. Mater. Chem. C*, 2024, **12**, 7981–7988.
- 214 Y. Sheng, H. Yang, Y. Wang, L. Han, Y. Zhao and A. Fan, *Talanta*, 2017, **166**, 268–274.
- 215 W. Liu, Y. Guo, H. Li, M. Zhao, Z. Lai and B. Li, *Spectrochim. Acta, Part A*, 2015, **137**, 1298–1303.
- 216 F. Liu, S. Wang, M. Zhang, Y. Wang, S. Ge, J. Yu and M. Yan, *Microchim. Acta*, 2014, **181**, 663–670.
- 217 Y. Wang, S. Wang, S. Ge, S. Wang, M. Yan, D. Zang and J. Yu, *Anal. Methods*, 2013, **5**, 1328–1336.
- 218 F. Li, L. Guo, Y. Hu, Z. Li, J. Liu, J. He and H. Cui, *Talanta*, 2020, **207**, 120346.
- 219 M. A. Tzani, D. K. Gioufthidou, M. G. Kallitsakis, N. V. Pliatsios, N. P. Kalogiouri, P. A. Angaridis, I. N. Lykakis and M. A. Terzidis, *Molecules*, 2021, **26**, 7664.
- 220 Y. Cao, M. Wu, Y. Cao, W. Zhu and Y. Zhou, *Chem.-Asian J.*, 2025, **20**, e202401282.
- 221 D. Grieshaber, R. MacKenzie, J. Vörös and E. Reimhult, *Sensors*, 2008, **8**, 1400–1458.
- 222 M. Z. H. Khan, M. R. Hasan, S. I. Hossain, M. S. Ahommed and M. Daizy, *Biosens. Bioelectron.*, 2020, **166**, 112431.
- 223 C. Wang, M. Liu, Z. Wang, S. Li, Y. Deng and N. He, *Nano Today*, 2021, **37**, 101092.
- 224 W. Dungchai, O. Chailapakul and C. S. Henry, *Anal. Chem.*, 2009, **81**, 5821–5826.
- 225 J.-M. Oh and K.-F. Chow, *Anal. Methods*, 2015, **7**, 7951–7960.
- 226 S. E. F. Kleijn, S. C. S. Lai, M. T. M. Koper and P. R. Unwin, *Angew. Chem., Int. Ed.*, 2014, **53**, 3558–3586.



- 227 D. K. Pattadar, J. N. Sharma, B. P. Mainali and F. P. Zamborini, *J. Phys. Chem. C*, 2019, **123**, 24304–24312.
- 228 S. Aralekallu and L. K. Sannegowda, in *Handbook of Nanomaterials for Sensing Applications*, ed. C. M. Hussain and S. K. Kailasa, Elsevier, 2021, pp. 589–629, DOI: [10.1016/B978-0-12-820783-3.00001-4](https://doi.org/10.1016/B978-0-12-820783-3.00001-4).
- 229 O. S. Ivanova and F. P. Zamborini, *J. Am. Chem. Soc.*, 2010, **132**, 70–72.
- 230 H. Ma, P. Gao, P. Qian and Y. Su, *J. Phys. Chem. C*, 2020, **124**, 3403–3409.
- 231 T. Xiao, J. Huang, D. Wang, T. Meng and X. Yang, *Talanta*, 2020, **206**, 120210.
- 232 F. Arduini, L. Micheli, D. Moscone, G. Palleschi, S. Piermarini, F. Ricci and G. Volpe, *TrAC, Trends Anal. Chem.*, 2016, **79**, 114–126.
- 233 S. Nantaphol, O. Chailapakul and W. Siangproh, *Anal. Chim. Acta*, 2015, **891**, 136–143.
- 234 E. Eksin, H. Torul, E. Yarali, U. Tamer, P. Papakonstantinou and A. Erdem, *Talanta*, 2021, **225**, 122043.
- 235 S. Cinti, E. Proietti, F. Casotto, D. Moscone and F. Arduini, *Anal. Chem.*, 2018, **90**, 13680–13686.
- 236 J. Lu, S. Ge, L. Ge, M. Yan and J. Yu, *Electrochim. Acta*, 2012, **80**, 334–341.
- 237 J. Yang, Y.-G. Nam, S.-K. Lee, C.-S. Kim, Y.-M. Koo, W.-J. Chang and S. Gunasekaran, *Sens. Actuators, B*, 2014, **203**, 44–53.
- 238 W. Li, L. Li, M. Li, J. Yu, S. Ge, M. Yan and X. Song, *Chem. Commun.*, 2013, **49**, 9540–9542.
- 239 L. Li, Y. Zhang, L. Zhang, S. Ge, H. Liu, N. Ren, M. Yan and J. Yu, *Anal. Chem.*, 2016, **88**, 5369–5377.
- 240 W. Zheng, K. Wang, H. Xu, C. Zheng, B. Cao, Q. Qin, Q. Jin and D. Cui, *Anal. Bioanal. Chem.*, 2021, **413**, 2429–2445.
- 241 F. Ma, Q. Zhang and C.-y. Zhang, *J. Mater. Chem. B*, 2020, **8**, 3488–3501.
- 242 H. Qi, Y. Peng, Q. Gao and C. Zhang, *Sensors*, 2009, **9**, 674–695.
- 243 G. Valenti, E. Rampazzo, S. Kesarkar, D. Genovese, A. Fiorani, A. Zanut, F. Palomba, M. Marcaccio, F. Paolucci and L. Prodi, *Coord. Chem. Rev.*, 2018, **367**, 65–81.
- 244 S. Boobphahom, M. Nguyet Ly, V. Soum, N. Pyun, O.-S. Kwon, N. Rodthongkum and K. Shin, *Molecules*, 2020, **25**, 2970.
- 245 J. Yan, M. Yan, L. Ge, S. Ge and J. Yu, *Sens. Actuators, B*, 2014, **193**, 247–254.
- 246 S. Wang, L. Ge, M. Yan, J. Yu, X. Song, S. Ge and J. Huang, *Sens. Actuators, B*, 2013, **176**, 1–8.
- 247 J. Yan, M. Yan, L. Ge, J. Yu, S. Ge and J. Huang, *Chem. Commun.*, 2013, **49**, 1383–1385.
- 248 L. Wu, C. Ma, L. Ge, Q. Kong, M. Yan, S. Ge and J. Yu, *Biosens. Bioelectron.*, 2015, **63**, 450–457.
- 249 M. Zhang, L. Ge, S. Ge, M. Yan, J. Yu, J. Huang and S. Liu, *Biosens. Bioelectron.*, 2013, **41**, 544–550.
- 250 C. Gao, M. Su, Y. Wang, S. Ge and J. Yu, *RSC Adv.*, 2015, **5**, 28324–28331.
- 251 E. Martínez-Periñán, C. Gutiérrez-Sánchez, T. García-Mendiola and E. Lorenzo, *Biosensors*, 2020, **10**, 118.
- 252 W. Miao, *Chem. Rev.*, 2008, **108**, 2506–2553.
- 253 E. M. Gross, M. S. Sujana and S. M. Snyder, *Bioanalysis*, 2016, **8**, 2071–2089.
- 254 L. Zhang, Y. Wang, C. Ma, P. Wang and M. Yan, *RSC Adv.*, 2015, **5**, 24479–24485.

